2008

Modeling and simulation of nanoparticle aggregation in colloidal systems

Sergiy Markutsya
Iowa State University

Modeling and simulation of nanoparticle aggregation in colloidal systems

by

Sergiy Markutsya

A thesis submitted to the graduate faculty

in partial fulfillment of the requirements for the degree of

MASTER OF SCIENCE

Major: Mechanical Engineering

Program of Study Committee:
Shankar Subramaniam, Major Professor
Rodney Fox
Dennis Vigil
Pranav Shrotriya

Iowa State University

Ames, Iowa

2008

TABLE OF CONTENTS

LIST OF TABLES

LIST OF FIGURES

ABSTRACT

Prediction of colloidal nanoparticle aggregation is an important problem which needs to be solved in an accurate and efficient manner. Thus, accurate modeling of physico-chemical interactions is required. In addition, to have good aggregation statistics, large system sizes should be considered, which can significantly increase computational cost and decrease code efficiency. In ideal case model which is chosen to predict colloidal nanoparticle aggregation should accurately describe physico-chemical interactions of relatively large physical systems, and at the same time, simulate at low computational cost.

In this research, two simulation approaches, molecular dynamics (MD) and Brownian dynamics (BD), are analyzed and compared with a view to accurately predicting aggregation of colloidal nanoparticles. Based on this comparison it was found that MD approach is not feasible to simulate an aggregation of colloidal nanoparticles for systems of physical sizes but can be used to simulate non-physical (model) systems. Thus, such coarse-grain approaches as BD have to be used instead. Because the BD technique is essentially a reduction of the MD method the accuracy requirements for BD simulations have been established.

Analysis of characteristic time scales for the BD approach justifies reduction of position and velocity-Langevin equations to position-Langevin for physical system and is not justified for model system.

A new method to match aggregation statistics obtained from MD and BD simulations is proposed in this work. In this method the evolution of the second-order density for MD model is derived. The average relative acceleration between nanopartilce pairs is identified as an important link between MD and coarse-grain simulations such as BD.

Although BD is a coarse-grain model with fewer degrees of freedom, it gives reasonable

predictions of nanoparticles aggregation. Also, because of its high computational efficiency this method can be a useful tool to simulate nanoparticle aggregation in colloidal systems.

CHAPTER 1. INTRODUCTION

Nanoparticles are widely used as building blocks in nanotechnology research. Because the size of nanoparticles scales to tens of nanometers, new materials in nanoscale range can be created. Moreover, properties of such materials differs from bulk material properties [1]. Mainly two high-rate synthesis methods are used in the industry: aerosol reactors in a gaseous environment and colloidal reactors in a fluid environment [1, 2]. In most of the methods the synthesis of the particles occurs due to the reaction of chemical precursors and the formation of nuclei, which rapidly grow due to surface addition and/or aggregation. The next generation of applications will require improvement in the quality of the monodispersity, purity, and uniform surface chemistry of nanoparticles [2]. Because the aggregation of the colloidal nanoparticles is the important part of this process, a better understanding of the aggregation process will help to improve synthesis methods.

Prediction of colloidal nanoparticle aggregation is an important problem which needs to be solved in an accurate and efficient manner. Thus, accurate modeling of physico-chemical interactions is required. This can be achieved by developing the coarse-grained particle interaction potentials derived from quantum mechanics calculations, that are suitable for large scale nanoparticle aggregation simulations. In this case, the atomic models for surface molecules of polystyrene nanoparticles can be developed to calculate surface-molecule, surface-surface, and molecule-molecule interaction forces. These results can be validated by atomic force microscopy (AFM) measurements of polystyrene-polystyrene nanoparticles, and used in simulation of nanoparticles aggregation as a physical potential.

In addition, to have good aggregation statistics, large system sizes should be considered, which can significantly increase computational costs and decrease code efficiency. Ideally the

model which is chosen to predict colloidal nanoparticle aggregation should accurately describe physico-chemical interactions of relatively large physical systems, and at the same time, simulate at a low computational cost. In reality this is hard to achieve. In many cases if the model is very accurate it is usually not efficient and cannot be used to simulate a physical problem. On the other hand, more efficient models usually are not very accurate in terms of representing the physics, thereby limiting their applicability. Thus, a computational model which is chosen to predict an aggregation of colloidal nanoparticles should maintain the balance between the level of accuracy and computational efficiency.

An accurate description of the colloidal nanoparticle aggregation process can be done by performing an accuracy analysis of the statistics which characterize aggregation. To completely characterize aggregation statistics such as the extent of aggregation ξ, cluster size distribution (CSD), and the radial distribution function $g(r)$ need to be analyzed. The extent of aggregation, $0 \leq \xi < 1$ is defined as

$$\xi = 1 - \frac{M_0(t)}{M_0(0)} \tag{1.1}$$

where M_0 is the zeros moment of the total concentration of clusters. This parameter represents the relative mass of aggregates in the system at time t. Therefore, this variable approaches unity when all the system mass accumulates in a single cluster. And $\xi = 0$ if monomers are staying separate and do not form clusters at all time. Knowledge of this parameter allows us to estimate the level of aggregation in a system. More detailed information about aggregation statistics can be obtained by analyzing CSD data. In this case, the number of clusters and their size distribution is obtained. This additional level of detail can be very important when accuracy of the computational model is under investigation. Even though the CSD gives information about cluster sizes, it does not give any information about cluster structure. Therefore, the radial distribution function $g(r)$ is introduced as an additional characteristic to provide information about the structure of clusters. Together these three parameters provide complete characterization of the aggregation process and all of them should be used when an accuracy analysis is performed.

For aggregating systems some additional parameters are often calculated, such as the cluster

radius of gyration R_g and the cluster fractal dimension D_f [3, 4, 5, 6]. The cluster radius of gyration defines the average size of the cluster, and the cluster fractal dimension is an indication of how completely a cluster appears to fill space. The mass of the cluster scales with geometric size as $N \sim R_g^{D_f}$ and by plotting $\log(N)$ versus $\log(R_g)$; linear regression yields a slope equal to D_f. The advantage of this method is a simplicity of D_f calculation. However, this method can be only used for the ensemble of clusters of different sizes and is not applicable for cases with fewer clusters in the system due to the statistical variation in the R_g values.

Light scattering analysis is proposed as another method for investigating aggregate structure [4, 5, 6]. This method allows measuring D_f even for a single cluster from the slope of the log-log plot of the structure factor of an aggregate $S(q)$ versus qa, where q is the scattering wave vector and a is the particle diameter. The light scattering technique gives cluster structure information for a wide range of scales: from monomer size to the geometric size of a cluster. This feature allows us to discover any possible structure changes at different length scales, especially for the relatively large clusters where it gives the most complete description of the aggregate structure. Also, this technique is very useful when an aggregation of the realistic physical system is investigated from an experimental and computational perspective. In this case, the light scattering technique allows direct comparison of the cluster structures for experimentally measured physical systems and computationally simulated systems. Thus, the validation process of the computational model simplifies significantly.

A major difficulty in the simulation of colloidal nanoparticles is the wide range of time and length scales which are present in the system. The wide range of time scales is introduced by the presence of short-time Brownian motion and the long-time hydrodynamic behavior of solvent. The wide range of length scales occurs due to the size separation of colloidal nanoparticles and solvent molecules. There are many simulation techniques that are commonly used to describe the dynamics of colloidal nanoparticle aggregation.

Molecular dynamics (MD) simulation is an established technique that can simulate colloidal nanoparticle aggregation [7]. In the MD approach, solute and solvent particles interact through a modeled, intermolecular potential, and the positions and velocities of these particles evolve in

time according to Newton's equations of motion. In most MD simulations, the intermolecular potential energy is taken to be the sum of isolated pair interactions, which is called the *pairwise additivity* assumption. The main difficulty with such an approach is that it can not be used to model aggregation of a realistic system of colloidal nanoparticles. The requirements of large size separation between nanoparticles and solvent molecules ($d_{NP} \sim 40$ nm, $d_{solv} \sim 0.3$ nm and $d_{NP}/d_{solv} \sim 100$ at solvent molecules volume fraction $\lambda_{solv} \sim 0.45$), and the large number of nanoparticles that are modeled to have good statistics of aggregated clusters lead to an enormous number of solvent molecules in the system (on the order of 10^{10}). Moreover, calculation of intermolecular forces between solvent molecules in MD would require to resolve time scales on the order of 10^{-15} s. Therefore, simulating any colloidal system even far from realistic physical parameters is a challenging and sometimes even impossible task. Alternative approaches are needed to resolve this problem. One alternative is to use approaches designed for nanoparticle aggregation simulation.

Based on the off-lattice Monte Carlo (OLMC) simulation, several methods are frequently used to model nanoparticle aggregation. These models include diffusion-limited aggregation (DLA), diffusion-limited cluster aggregation (DLCA), ballistic-limited aggregation (BLA), ballistic-limited cluster aggregation (BLCA), reaction-limited aggregation (RLA), and reaction-limited cluster aggregation (RLCA).

In DLA models, particles diffuse through a random-walk from distant points and finally arrive and stick to the surface of the growing aggregate [8, 9]. In the DLCA model, the particles and clusters move in random-walk trajectories, which represent the Brownian motion of the particles and clusters in a dense fluid [10, 11]. According to this model, particles and aggregates are moved randomly, and when the distance between centers of two particles approach "cluster distance" r_{cl} (the maximum distance between two neighbor particles which belong to the same cluster) they irreversibly link. After this linking if the distance between any pair of particles in two different clusters appears to be less than r_{cl}, two clusters move apart along their approach path until the separation is equal to the cluster distance. Thus, stickiness probability p_{stick} for these two approaches is unity. DLCA is the more appropriate model when

simulating colloidal aggregation because in reality, aggregates grow not only due to cluster-monomer interaction but also due to the cluster-cluster interaction. Both DLA and DLCA models allow simulating the aggregation of systems with more than a million nanoparticles, which gives good statistics of aggregates. However, these approaches can only be applied if the interparticle interactions are smaller than $k_B T_{ref}$, where k_B is the Boltzmann constant and T_{ref} is the reference temperature. If the interactions are large compared with $k_B T_{ref}$ for some length scale l, the structure of the resulting aggregates will be changed over this length scale, and fractal dimensionality may be changed if the interactions are sufficiently strong [12].

In BLA models, particles and clusters are added to each other through linear paths. Each path is chosen randomly from all possible paths that could result in a collision between the particle and cluster [13]. Similarly, the BLCA approach models cluster-cluster collisions in addition to the particle-cluster collision used in BLA [14]. BLA and BLCA approaches were developed in the 1960s. These models were used because at that time it was not sufficiently efficient to carry out simulations with random walk trajectories which are implemented in DLA and DLCA models. The use of BLA and BLCA approaches for colloidal nanoparticle aggregation modeling is limited due to the assumption of linear paths between collisions, which can lead to incorrect cluster size distributions.

In RLA and RLCA models, particles and clusters (just particles in the RLA case) follow random walk trajectories, but they do not form a new cluster each time they come into contact [15]. Instead, they continue their random walk paths and many collisions are usually required before a pair of clusters will join. This behavior is dictated by the presence of a repulsive barrier in the particle-particle pair potential. Only when this barrier is overcome will the short-range attractive force finally hold two clusters together. This process is identical to DLA and DLCA models with a small sticking probability p_{stick}. A disadvantage of this method is the very large amount of computer time required if the sticking probability is small.

All the models represented above help to characterize complicity of aggregate structures by extracting important characteristics, such as the size distribution of aggregating clusters, dimensionality of the cluster structure, and local concentration of the particles in the sys-

tem in very efficient way. However, there are several weak points in using these models for nanoparticles aggregation:

i. With these models it is impossible to use interaction potentials which can be derived from quantum mechanics calculations for a realistic physical system.

ii. All these models imply an irreversible linking of particle-cluster and cluster-cluster when new clusters are formed. This prohibits rearrangement of nanoparticles within a cluster as well as dissociation of one cluster into two or more. This will give incorect results in aggregation structure, especially when nanoparticle aggregation with shear force is simulated.

iii. A structure of clusters obtained with these models depends on model parameter such as cluster distance r_{cl}, which makes it impossible to implement any of these models for the dynamic simulation of the colloidal nanoparticle aggregation.

To overcome these problems and keep simulation efficiency it is also proposed to use off-lattice Dynamic Monte Carlo simulation (DMC) [16]. However, it can be used only for some limited cases.

Another alternative to MD simulations are coarse-grained models. There is a wide variety of coarse-grained simulation techniques to model the dynamics of colloidal suspensions. Among these techniques the Brownian dynamics (BD) technique is the most frequently used to simulate diffusion problems. On the other hand such techniques as dissipative particle dynamics (DPD), and stochastic rotational dynamics (SRD) are most advanced one.

Dissipative particle dynamics [17, 18] is an alternative to standard MD techniques and includes hydrodynamic and Brownian fluctuations. In DPD, fluid molecules themselves are not represented, but instead, groups of molecules called dissipative particles are considered. These dissipative particles are simulated to obtain a flow field. These dissipative particles interact with each other dissipatively, exchange momentum, and move randomly like Brownian particles. The main advantage of DPD is that in this method the multibody hydrodynamic interactions among colloidal particles are automatically reproduced through the interactions

with dissipative particles. However, even though the number of dissipative particles in DPD is less than in MD, this method is still computationally expensive, because the dissipative particles still interact through the pairwise potentials and the number of colloid nanoparticles N_p is much smaller than the number of dissipative particles N_{dp}.

In the SRD approach [19], all the space in SRD is partitioned using a rectangular grid. Nanoparticles and solvent particles move in continuous space according to Newton's laws of motion, excluding solvent-solvent interaction. This excluded interaction is modeled by collision events at discrete times called collision time steps. At these collision events, solvent particles inside each cell exchange momentum by rotating their velocity vector relative to the center of mass velocity of the cell around a randomly chosen axis. This method is more efficient than MD because there is no direct computation of solvent-solvent interactions; but instead this solvent-solvent collision is simulated at every collision step which is much greater than the computational time step. This method successfully models aggregation of colloidal nanoparticles [20].

In the BD approach, [21] it is assumed that the collisions of colloidal nanoparticles with solvent molecules induce their random displacement. As a result, the positions and velocities of the colloidal nanoparticles change accordingly. In BD the local momentum is not conserved; however, it satisfies the average momentum conservation (ensemble average). This approach is very attractive for simulation of colloidal nanoparticle aggregation due to its simplicity and efficiency [22]. In the present work Brownian dynamics method will be described and analyzed in detail with respect to the aggregation of colloidal nanoparticles.

The objective of this work is to:

1. Validate and verify a Brownian dynamics code,

2. Compare aggregation statistics for BD and MD simulations,

3. Propose a method to better match BD aggregation statistics with MD.

In Chapter 2, the MD model is described and its feasibility for simulation of realistic physical systems is discussed. In Chapter 3, the validation of BD is discussed together with

error analysis and aggregation regime map analysis. Chapter 4 describes the results from the simulation of aggregating systems obtained from MD and BD models. Light scattering analysis of the aggregate systems is introduced to extract aggregation statistics. In Chapter 5, an improved model of aggregating systems is represented and discussed. The conclusions of this study and recommendations for future work are discussed in Chapter 6.

CHAPTER 2. SIMULATION OF MOLECULAR DYNAMICS

In this chapter, the molecular dynamics method is described, and its applicability to the modeling of aggregation of colloidal nanoparticles in physical systems is discussed.

2.1 Molecular Dynamics Model

Atomistic simulation methods such as MD can, in principle, provide the detailed information concerning collision, aggregation, and breakage events that is needed to derive realistic expressions for aggregation (and breakage) rate kernels, because they explicitly represent all molecules in the system (both solute and solvent). The motion of these molecules is computed using classical Newtonian mechanics [23]:

$$d\mathbf{r}_i = \mathbf{v}_i dt \tag{2.1}$$

$$d\mathbf{v}_i = \frac{1}{m_i}\mathbf{F}_i(\{\mathbf{r}\})dt, \qquad i = 1, \ldots, N \tag{2.2}$$

where $N = N_s + N_p$ is the total number of particles in a system, N_s is the number of solute particles, N_p is the number of nanoparticles, m_i is the mass of i-th particle, dt is the computational time step, $\mathbf{r}_i$ is the position of i-th particle, and $\mathbf{v}_i$ is the velocity of i-th particle. The force $\mathbf{F}_i(\{\mathbf{r}\})$ is determined as the force which acts on i-th particle due to the remaining $(j = 1, \ldots, N-1)$ particles. By assuming pairwise additivity, this force is calculated as

$$\mathbf{F}_i = \sum_{j=1, j\neq i}^{N} \mathbf{F}_{ij}(\mathbf{r}_{ij}) \tag{2.3}$$

where $\mathbf{r}_{ij}$ is the pair separation between i-th and j-th particles, and $\mathbf{F}_{ij}(\mathbf{r}_{ij})$ is the force that acts on particle i due to presence of particle j. By considering the fact that the total number of particles in a system consists of solvent particles and nanoparticles $(N = N_s + N_p)$, Eq.2.3

can be rewritten as

$$\mathbf{F}_i^{\beta} = \sum_{j=1}^{N_\gamma} \mathbf{F}_{ij}^{\beta\gamma}(\mathbf{r}_{ij}) + \sum_{k=1,k\neq i}^{N_\beta} \mathbf{F}_{ik}^{\beta\beta}(\mathbf{r}_{ik}) \tag{2.4}$$

where $\beta, \gamma = s, p$ are the indices for solvent and/or nanoparticles.

To compute forces in Eq.2.4 it is necessary to define force laws between each type of molecule (*e.g.*, nanoparticle-nanoparticle, nanoparticle-solvent, and solvent-solvent). Typically these forces are obtained by differentiating presumed intermolecular potential energy functions (such as the well-known Lennard-Jones potential) fitted to experimental data. These presumed potential energy functions mimic the competition between near-range repulsions arising from the overlap of electronic shells and long-range attractive Van der Waals forces. Hence, interaction potentials typically display a potential energy minimum at intermediate distances that arises from the balance of the longer-range attractive forces and short range repulsive forces. More recently, there have been efforts to avoid the use of presumed interaction potentials by instead using coarse-graining procedures to compute these interaction potentials with information obtained from quantum mechanical calculations [24, 25].

Even when accurate pairwise interaction potentials are available, other problems with using the MD approach for simulation of aggregation of colloidal nanoparticles remain. For real colloids there is a size separation of nanoparticles and solvent molecules. Due to this separation in scales between the sizes of the solvent molecules (typically $10^{-10} - 10^{-9}$ m) and nanoparticle aggregates (usually $10^{-8} - 10^{-7}$ m), an enormous number of solvent molecules is required for a simulation, especially for dilute systems. To investigate the influence of the nanoparticle/solvent size separation on the calculation speed, a simple test is carried out. In this test, two sets of MD simulations are carried out under identical conditions except for the nanoparticle/solvent diameter ratio used (equal nanoparticle and solvent sizes in one case, and nanoparticle's diameter twice that of the solvent in the other case). Results of this test, plotted in Figure 2.1, show that the CPU time required for each simulation time step as a function of the number of molecules simulated using the MD simulation software LAMMPS [26].

It is readily apparent that the CPU time scales approximately linearly with the number of

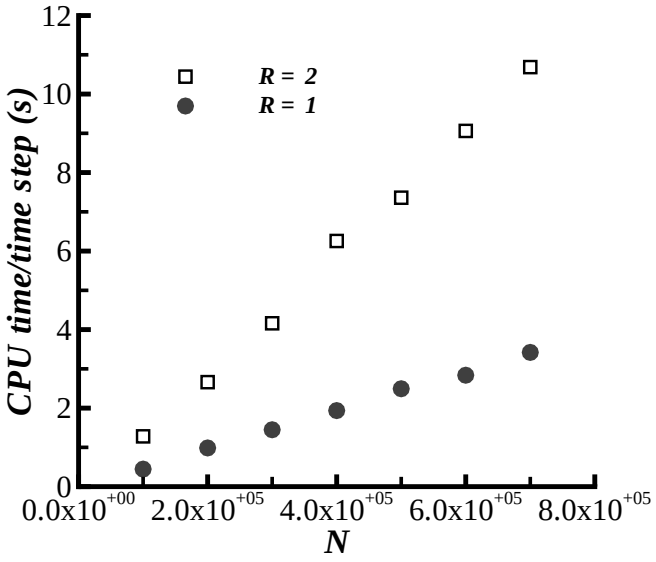

Figure 2.1 Dependence of MD simulation CPU time on the total number of Lennard-Jones particles, N, and the nanoparticle/solvent diameter ratio, R for non-aggregating particles. All other simulation parameters are identical in the two sets of simulations. Nanoparticle volume fraction is 0.005.

molecules, but that the CPU time grows more rapidly with the increasing nanoparticle/solvent size ratio. A typical realistic simulation would require nanoparticle/solvent size ratios on the order of at least 10-100; therefore it is evident that MD simulation of aggregation, even when using nano-scale primary particles, is computationally demanding. An estimation of the time needed for the MD simulation of a system with nanoparticle/solvent size ratio equal to 14 and containing only 31 nanoparticles is given in Table 2.1. These results clearly show that in order to simulate just a few nanoparticles of 4 nm diameter on 20 processors will take more than 100 days of CPU time. Furthermore, the dynamic range of the largest aggregates to the primary nanoparticles can itself be two to three orders of magnitude in light-scattering experiments [27]. Hence, to obtain a meaningful statistical distribution of aggregates, it is clear that very large systems will need to be simulated. All these factors contribute to the conclusion that MD simulation of aggregation with existing simulation packages and hardware is computationally prohibitive. Therefore, coarse-grained models, such as Brownian dynamics

Table 2.1 Estimation of MD simulation time for 31 non-aggregating nanoparticles. All solvent and nanoparticle interactions were modeled using Lennard-Jones potentials with well depth ε and particle radius σ. The time increment is fixed at 5×10^{-15} sec.

Parameters	Solvent	Nanoparticles
σ (m)	2.85×10^{-10}	4.0×10^{-9}
m (kg)	1.33×10^{-26}	3.686×10^{-23}
ε (kg-m^2/s^2)	1.073×10^{-21}	1.646×10^{-20}
N	146,840	31
time steps/CPU sec (1 processor)	0.06	
CPU time for 10^7 steps (20 processors)	115 days	

must be used instead.

CHAPTER 3. SIMULATION OF BROWNIAN DYNAMICS

Brownian Dynamics (BD) is a coarse-grained model that is successfully used to model diffusion of solute particles in a solvent bulk [28]. In this model only N_p nanoparticles are considered with no implicit simulation of N_s solvent molecules which significantly speeds up the simulations. Several investigators have employed the BD approach to simulate particle aggregation [29]-[34]. However, there are no systematic efforts to establish the accuracy and validity of this approach for the aggregation of colloidal nanoparticles. In this chapter, the governing equations for the BD approach are analyzed and their numerical solutions for two sets of parameters which correspond to modeling system and physical system are discussed. For these systems, the applicability of reduction from position and velocity to the position-Langevin equation is analyzed based on the relative magnitude of the characteristic times. In addition, an analysis of parameters that have a significant influence onto colloidal nanoparticle aggregation is performed. And finally, the requirements for numerical convergence and the accuracy of the BD simulations for colloidal nanoparticle aggregation is established.

3.1 Position and Velocity-Langevin Evolution Equation

In the Brownian dynamics method, the nanoparticle-nanoparticle interactions are incorporated into Langevin equations for nanoparticles only with no need to track solvent molecules explicitly. The position $\mathbf{r}_i$ and velocity $\mathbf{v}_i$ of the i-th nanoparticle are incremented over a time step dt by position and velocity-Langevin equations:

$$d\mathbf{r}_i = \mathbf{v}_i dt \tag{3.1}$$

$$d\mathbf{v}_i = -\gamma \mathbf{v}_i dt + \frac{1}{m_i}\mathbf{F}_i(\{\mathbf{r}\})dt + \underline{\underline{\mathbf{B}}} d\mathbf{W}_i \tag{3.2}$$

In this equation, $\gamma = \sigma_{v_\infty}^2/D_\infty$ is the friction coefficient, $\sigma_{v_\infty}^2 = k_B T_{ref}/m_i$ is the velocity variance, m_i is the mass of i-th particle, k_B is the Boltzmann constant, T_{ref} is the reference temperature, and D_∞ is the diffusion coefficient of a nanoparticle in the solvent in the infinite dilution limit. $\underline{\underline{\mathbf{B}}}$ is the matrix of constants which is $\underline{\underline{\mathbf{B}}} = \Sigma_v \underline{\underline{\mathbf{I}}}$ for an isotropic system, $\underline{\underline{\mathbf{I}}}$ is 3×3 identity matrix, $\Sigma_v = \sqrt{2\gamma\sigma_{v_\infty}^2}$ is a constant, and $d\mathbf{W}_i$ is the Wiener process increment. The force $\mathbf{F}_i(\{\mathbf{r}\})$ is the systematic net force on the i-th nanoparticle due to its interaction with all other $(N_p - 1)$ nanoparticles. With pairwise additive assumption this force is calculated as

$$\mathbf{F}_i = \sum_{j=1, j\neq i}^{N_p} \mathbf{F}_{ij}(\mathbf{r}_{ij}) \tag{3.3}$$

where $\mathbf{r}_{ij}$ is the pair separation between i-th and j-th particles, and $\mathbf{F}_{ij}(\mathbf{r}_{ij})$ is the force that acts on particle i due to presence of particle j, which is related to $\mathbf{F}_{ik}^{\beta\beta}(\mathbf{r}_{ik})$ in Eq.2.4 with $\beta = p$. Frictional and random force components in Eq.3.2 represent $\mathbf{F}_{ij}^{\beta\gamma}(\mathbf{r}_{ij})$ in Eq.2.4 with $\beta, \gamma = s, p$.

Langevin equations 3.1 and 3.2 do not describe a hydrodynamic effect. Hydrodynamic effect can be introduced through the considering $6N_p \times 6N_p$ diffusion tensor $\underline{\underline{\mathbf{D}}}$ around a point particle subject to a force [35], where N_p is the number of nanoparticles in a system. The diffusion tensor can be partitioned into four $3N_p \times 3N_p$ sub matrices:

$$\underline{\underline{\mathbf{D}}} = \begin{bmatrix} \underline{\underline{\mathbf{D}}}^t & \underline{\underline{\mathbf{D}}}^{cT} \\ \underline{\underline{\mathbf{D}}}^c & \underline{\underline{\mathbf{D}}}^r \end{bmatrix} \tag{3.4}$$

where $\underline{\underline{\mathbf{D}}}^t$ is the transitional matrix, $\underline{\underline{\mathbf{D}}}^r$ is the rotational matrix, and $\underline{\underline{\mathbf{D}}}^c$ is the coupling matrix (T denotes the matrix transpose). The matrix $\underline{\underline{\mathbf{D}}}$ is related to the grand friction matrix $\underline{\underline{\gamma}}$ by the generalized Einstein equation:

$$\underline{\underline{\mathbf{D}}} = k_B T \underline{\underline{\gamma}}^{-1} \tag{3.5}$$

The translational and rotational frictional coefficients for a spherically isotropic particle of radius a are defined based on the stick or slip boundary conditions. Stick boundary conditions are correct for large, solid, and impermeable particles immersed in a viscous medium. In this case two scalar friction coefficients take the form

$$\gamma^t = 6\pi\eta a, \quad \gamma^r = 8\pi\eta a^3 \tag{3.6}$$

where η is the Newtonian viscosity of the medium. In case of a smooth spherical particle, the perfect slip occurs, and the friction coefficients are

$$\gamma^t = 4\pi\eta a, \quad \gamma^r = 0 \tag{3.7}$$

For a particle of infinite viscosity η_p immersed in an unbounded continuum of viscosity η_0 the value for the transitional friction coefficient can be estimated by

$$\gamma^t = 2\pi\eta a \left[3 + \frac{2\eta_0}{\eta_p}\right] \left[1 + \frac{\eta_0}{\eta_p}\right]^{-1} \tag{3.8}$$

According to Oseen formulation the translational diffusion is described as

$$\mathbf{D}_{ii} = \frac{k_B T}{6\pi\eta a}\underline{\underline{\mathbf{I}}} \tag{3.9}$$

$$\mathbf{D}_{ij} = \frac{k_B T}{8\pi\eta r_{ij}} \left[\underline{\underline{\mathbf{I}}} + \frac{\mathbf{r}_{ij} \cdot \mathbf{r}_{ij}}{r_{ij}^2}\right] \tag{3.10}$$

where $\mathbf{r}_{ij} = \mathbf{r}_i - \mathbf{r}_j$ is the separation of i-th and j-th particles. This formulation is appropriate for stick boundary conditions with point sources of friction. In case of finite particle size the equation of Rotne and Prager can be used

$$\mathbf{D}_{ii} = \frac{k_B T}{6\pi\eta a}\underline{\underline{\mathbf{I}}} \tag{3.11}$$

$$\mathbf{D}_{ij} = \frac{k_B T}{8\pi\eta r_{ij}} \left\{ \left[\underline{\underline{\mathbf{I}}} + \frac{\mathbf{r}_{ij} \cdot \mathbf{r}_{ij}}{r_{ij}^2}\right] + \frac{2a^2}{3r^2} \left[\underline{\underline{\mathbf{I}}} - \frac{3\mathbf{r}_{ij} \cdot \mathbf{r}_{ij}}{r_{ij}^2}\right] \right\} \tag{3.12}$$

Thus, by introducing hydrodynamic effect into BD model, the simulation time significantly increases which can negate all the advantages of BD in comparison with MD approach. In many cases hydrodynamic effects are not significant when modeling relatively large ($\sim 10 - 40nm$) colloidal nanoparticles in fluid and may not be taken into account.

The advantage of using BD simulations instead of MD simulations in terms of computational cost is evident by comparing data in Table 2.1 and Table 3.1, where estimates of the execution time for MD and BD simulations of identical system of nanoparticles are given. In particular, a comparison of the number of simulation time steps executed per second of CPU time demonstrates that there is more than three orders of magnitude speedup in the BD simulations as a result of the fact that individual solvent molecules are not simulated, and

Table 3.1 Estimation of BD simulation time for 31 non-aggregating nanoparticles. All nanoparticle interactions were modeled using Lennard-Jones potentials with well depth ε and nanoparticle diameter σ. The time increment is fixed at 5×10^{-15} sec.

Parameters	Nanoparticles
σ (m)	4.0×10^{-9}
m (kg)	3.686×10^{-23}
ε (kg-m^2/s^2)	1.646×10^{-20}
N	31
time steps/CPU sec (1 processor)	100
Time for 10^7 steps (20 processors)	2 hrs

positions and velocities are calculated only for the nanoparticles. This speedup is a necessity for simulating aggregation in colloidal systems, where the number of nanoparticles and the aggregate sizes are relatively large.

By analyzing a homogeneous system of nanoparticles which is described by the Langevin equation (3.2), two characteristic time scales can be identified. One is a velocity relaxation time τ_γ that is related to the frictional part, and the other time scale τ_F is related to the systematic force. These time scales are

$$\tau_\gamma = \frac{1}{\gamma} = \frac{D_\infty}{\sigma_{v_\infty}^2}, \tag{3.13}$$

and

$$\tau_F = \frac{m\sigma\sigma_{v_\infty}}{\varepsilon}. \tag{3.14}$$

In these equations $\sigma_{v_\infty}^2 = k_B T_{ref}/m$ is the velocity variance, σ is the nanoparticle diameter, and ε is the well depth of the interaction potential between nanoparticles.

Different algorithms can be used to integrate Eqs. (3.1) and (3.2) based on the relative magnitudes of the characteristic time scales and the computational time step Δt. A velocity relaxation time scale τ_γ characterizes a momentum relaxation in the system, when τ_F characterizes a configuration relaxation. When the velocity relaxation time is smaller than the

configuration relaxation time ($\tau_\gamma < \tau_F$), then the algorithms proposed by Allen [36] and Van Gunsteren [37] can be used. When the velocity relaxation time and the configuration relaxation time are of the same order of magnitude ($\tau_\gamma \sim \tau_F$), then the algorithm proposed by Turq *et al.* [38] is applicable. And finally, if the configuration relaxation time is much greater than the velocity relaxation time ($\tau_\gamma \ll \tau_F$), then the algorithm, proposed by Ermak and McCammon [39] can be applied. For all these cases the computational time step Δt is determined solely by the value of the frictional time scale such that ($\Delta t < \tau_F$) [28].

For the last case, where the momentum relaxation time is short in comparison with the configuration relaxation time (which includes most of the cases for particles suspended in liquids), the system of equations (3.1)-(3.2) can be reduced to one position-Langevin (PL) equation [39]:

$$d\mathbf{r}_i = \frac{\mathbf{F}(\{r_i\})}{m_i\gamma}dt + \frac{\Sigma_v}{\gamma}d\mathbf{W}_i. \tag{3.15}$$

Such a reduction of position and velocity-Langevin equations into one position-Langevin equation significantly simplifies the BD model where only the position of nanoparticles is tracked.

3.2 BD Simulation of Model and Physical Systems

Accurate and efficient simulation of the aggregation of colloidal nanoparticles for systems of realistic sizes is the goal of this work. Therefore, there is an interest in simulation of physical systems with BD. On the other hand, for the purpose of code verification there is a need for comparison of the BD simulation with MD. Because MD cannot simulate systems of realistic sizes (which is discussed in the previous Chapter), for the purposes of comparison of MD and BD simulation results, model systems are also used with BD approach. Therefore, both model systems and physical systems are considered.

In all the simulations, the dimensional quantities are scaled to correspondent non-dimensional counterparts. This approach allows direct comparison of different physical systems. Thus, it is quite possible that systems with different physical parameters will have the same non-

dimensional form which is a sign of a self-similarity of two different systems. Table 3.2 lists all the characteristic parameters which are used in the present work.

Table 3.2 Characteristic dimension and reduced parameters used in the present work.

Parameter	Dimension	Description
σ	Length	Particle size
ε	Energy	Interaction potential well depth
m	Mass	Particle mass
T_∞	Temperature	Reference temperature
α	N/A	Volume fraction
d	N/A	Dimension of physical space
$\hat{r} = \frac{r}{\sigma}$	N/A	Reduced distance
$\hat{t} = t\frac{\sigma_{v_\infty}}{\sigma}$	N/A	Reduced time
$\hat{\lambda} = \lambda\sigma^d$	N/A	Reduced number density
$\hat{\varepsilon} = \frac{\varepsilon}{k_B T_\infty}$	N/A	Reduced interaction potential well depth
$\hat{A} = A\frac{\sigma m}{\varepsilon}$	N/A	Reduced acceleration

When introducing model and physical systems into BD simulations, a self similarity question arises, because it is not clear if physical systems can be treated as model ones in BD simulation. Also, the question of possibility of PVL to PL reduction for model and physical systems should be answered. To clarify all of these questions, two sets of parameters which correspond to the model system and physical system are generated and represented in Table 3.3. Parameters for the physical system are chosen to be as close as possible to the real exper-

Table 3.3 Model system and physical system parameters

	***Model* system**	***Physical* system**
$\sigma(nm)$	0.34	4.00
m (kg)	3.32E-24	3.52E-23
$\hat{\varepsilon}$	8.0	8.0
α	0.005	0.005
N_p	10,000	35,000

imental setup, whereas parameters for the model system are chosen to be suitable for use in MD simulation.

In Table 3.3, $\hat{\varepsilon}$ is the non-dimensional well depth, which is defined in Table 3.2, α is the volume fraction of nanoparticles, and N_p is the number of nanoparticles in the system. The main difference between model and physical systems is in the diameter and mass of the nanoparticles, the diameter of nanoparticles being 12 times larger for the physical system.

Based on the parameters given in Table 3.3, the characteristic time scales were calculated using Eqs. 3.20 and 3.21. The results of these calculations for the model system and the physical system are given in Table 3.4.

Table 3.4 Characteristic times for model and physical systems

	***Model* system**	***Physical* system**
$\hat{\tau}_\gamma$	0.800	0.003
$\hat{\tau}_F$	0.125	0.125
$\hat{\tau}_F/\hat{\tau}_\gamma$	0.156	41.7

From Table 3.4 it can be seen that the model system $\hat{\tau}_\gamma \sim \hat{\tau}_F$, does not allow a PVL to PL reduction. At the same time, the non-dimensional timescales for the physical system are related as $\hat{\tau}_\gamma \ll \hat{\tau}_F$, which validates the PVL to PL reduction. Therefore, from an analysis of characteristic timescales for model and physical systems it is possible to conclude that PVL to PL reduction is prohibited for the model system. At the same time, for the physical system, the PVL to PL reduction is allowed.

3.2.1 Comparison of Computational Data for Model and Physical Systems

In order to make definitive conclusions about the applicability of the PVL to PL reduction for model and physical systems, the results obtained from the time scales analysis are verified by performing computational tests. For this purpose, both model and physical systems are simulated with BD by using PVL (Eqs. 3.1 and 3.2) and PL (Eq. 3.15) approaches with parameters described in Table 3.3 and Table 3.4.

If then PL is applicable for a particular system it should yield the same aggregation statistics (such as radial distribution function (RDF), mean square displacement (MSD), and cluster size distribution (CSD)) as PVL. Thus, to have a right aggregation, both the radial distribution function $g(r)$ and the mean square displacement $\langle r^2 \rangle$ should be described correctly and simultaneously. Also, one more parameter such as cluster size distribution is used to perform an additional control for the aggregation structure. So, these aggregation statistics are computed from PVL and PL BD simulations to conclude whether these approaches are equivalent for model and physical systems.

The radial distribution function is calculated according to the expression

$$g(r) = \frac{N(r, \Delta r)}{\frac{1}{2}\lambda N V(r, \Delta r)}. \tag{3.16}$$

where $N(r, \Delta r)$ is the number of particles found in a spherical shell (in 3-d case) of radius r and thickness Δr, $V(r, \Delta r)$ is the volume of spherical shell, and λ is the number density. $N(r, \Delta r)$ is defined as

$$N(r, \Delta r) = \sum_{i}^{N} \sum_{i<j}^{N} \delta(r - r_{ij}) \Delta r. \tag{3.17}$$

The mean square displacement is calculated as

$$\langle r^2(t) \rangle = \frac{1}{N} \sum_{i=1}^{N} \left(r_i(t) - r_i(0) \right)^2. \tag{3.18}$$

According to the analysis of characteristic time scales, the PVL to PL reduction for the model system is not justified. This conclusion is completely verified by the computational results. Even though the $g(r)$ is the same for PVL and PL for model system (Figure 3.1), the

mean square displacement (Figure 3.2) and cluster size distribution (Figure 3.3) are significantly different.

However, when the same simulations are performed for the physical system for which, according to the analysis, the PVL to PL reduction is justified, there is a perfect match of PVL and PL results for all three quantities, as is shown on Figures 3.4, 3.5, and 3.6.

The major results from the BD verification test are that

i. For the physical system, there is a sufficient separation of time scales exists ($\hat{\tau}_F/\hat{\tau}_\gamma \sim 42$) which allows the PVL to PL reduction. At the same time, for the model system, no time-scale separation exists ($\hat{\tau}_F/\hat{\tau}_\gamma \sim 0.2$), and therefore the PVL to PL reduction is not justified.

ii. Introduction of the other terms in (3.1) and (3.2) (such as shear force, etc.), will introduce an additional timescale which should be taken into account when the PVL to PL reduction is considered.

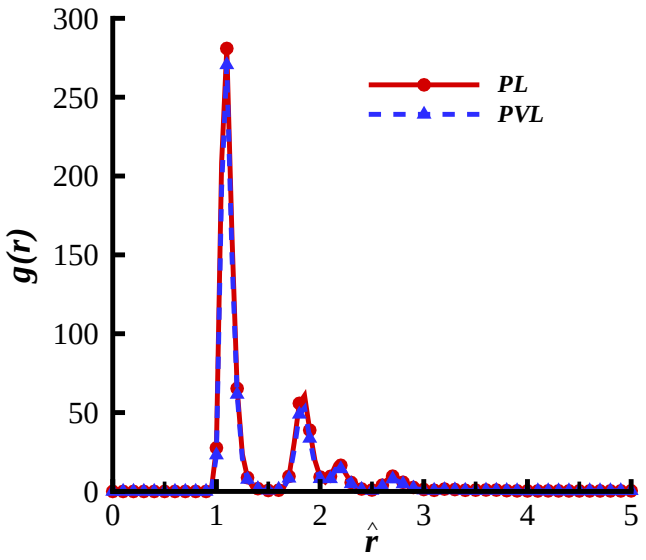

Figure 3.1 Radial distribution functions computed from PVL and PL BD simulations for the model system at $\hat{t} = 329.8$.

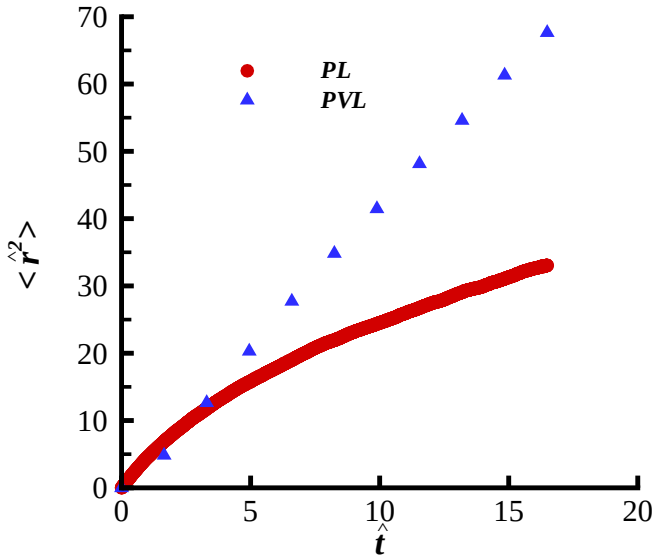

Figure 3.2 Mean square displacements computed from PVL and PL BD simulations for the model system.

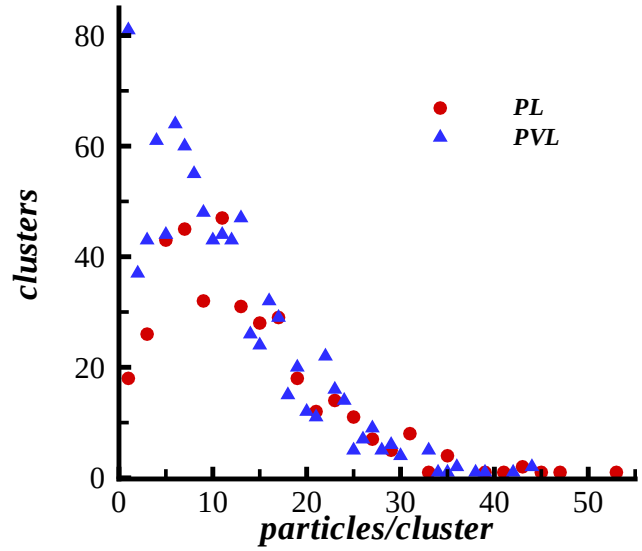

Figure 3.3 Cluster size distributions computed from PVL and PL BD simulations for the model system at $\hat{t} = 329.8$.

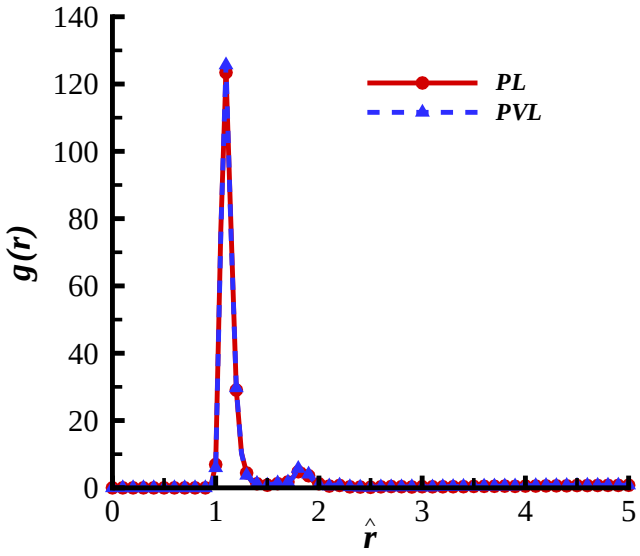

Figure 3.4 Radial distribution functions computed from PVL and PL BD simulations for the physical system at $\hat{t} = 675.8$.

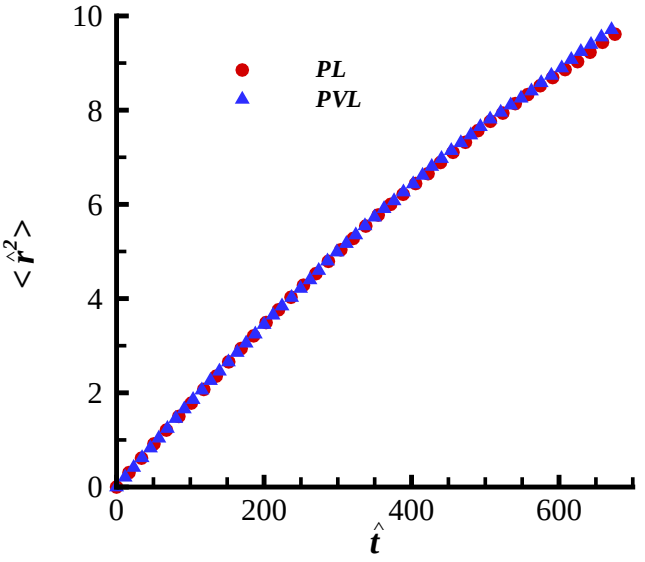

Figure 3.5 Mean square displacements computed from PVL and PL BD simulations for the physical system.

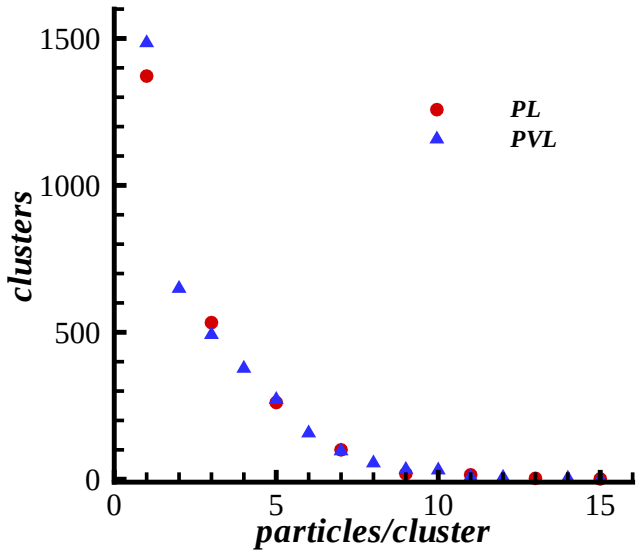

Figure 3.6 Cluster size distributions computed from PVL and PL BD simulations for the physcical system at $\hat{t} = 675.8$.

3.3 Aggregation Regime

In principle, given sufficient computational power and memory, converged BD simulations of aggregation can be executed if pair wise particle interaction potentials are known. However, it is not necessarily the case that significant aggregation will always occur in these systems, depending upon the system parameters. In this section, two important non-dimensional parameters are used to characterize clustering outcomes and thereby delineate a criterion for aggregation to occur in BD simulations.

In the BD model there are three parameters that play an important role in the aggregation, such as reduced potential well depth $\hat{\varepsilon}$, described in Table 3.2, reduced diffusivity $\hat{D}_\infty$, and the nanoparticle volume fraction α (see Appendix A for details). The reduced diffusivity is defined as

$$\hat{D}_\infty = \frac{D_\infty}{\sigma}\sqrt{\frac{m}{k_B T_\infty}} = \frac{D_\infty}{\sigma \sigma_{v_\infty}}. \tag{3.19}$$

The particle volume fraction is considered to be very low for the systems of interest in this study ($< 1\%$ by volume), so the variation in this parameter is neglected. The product $\hat{\varepsilon}\hat{D}_\infty$

can be interpreted as the ratio of the frictional and systematic force time scales. This can be shown by rewriting frictional and systematic force time scales (Eqs. 3.20 and 3.21) in a non-dimensional form according to Table 3.2

$$\hat{\tau}_\gamma = \frac{D_\infty}{\sigma_{v_\infty}^2}\frac{\sigma_{v_\infty}}{\sigma} = \frac{D_\infty}{\sigma\sigma_{v_\infty}} = \hat{D}_\infty, \tag{3.20}$$

and

$$\hat{\tau}_F = \frac{m\sigma\sigma_{v_\infty}}{\varepsilon}\frac{\sigma_{v_\infty}}{\sigma} = \frac{m\sigma_{v_\infty}^2}{\varepsilon} = \frac{m\frac{k_B T_\infty}{m}}{\varepsilon} = \frac{k_B T_\infty}{\varepsilon} = \frac{1}{\hat{\varepsilon}}. \tag{3.21}$$

Thus,

$$\hat{\varepsilon}\hat{D}_\infty = \frac{\hat{\tau}_\gamma}{\hat{\tau}_F}. \tag{3.22}$$

Therefore, if $\hat{\varepsilon}\hat{D}_\infty \ll 1$ (as is the case for nanoparticles suspended in liquids) there is sufficient separation in time scales such that the BD simulations can be carried out using a PL Langevin scheme obtained by integrating Eq. 3.2 [39].

In order to quantify the clustering of particles, we calculate the extent of aggregation, $0 \leq \xi < 1$, defined as

$$\xi = 1 - \frac{M_0(t)}{M_0(0)}. \tag{3.23}$$

where M_0 is the zeros moment or total concentration of clusters. Hence ξ is an aggregation progress variable that approaches unity as the system mass accumulates in a single cluster and equal to zero when nanoparticles are staying separate and do not form clusters at all time. Three-dimensional Brownian dynamics simulations were carried out using our in-house BD code to evolve $10,000$ primary particles with random non-overlapping initial positions. Particle-particle interactions were modeled by Lennard-Jones potentials, and simulations were continued until the clustering index ξ approached steady state. Other simulation details are provided in Table 3.5. Simulations were carried out for several fixed values of $\hat{\varepsilon}\hat{D}_\infty$, and the results are shown in Figure 3.7. It is evident that the extent of aggregation depends most sensitively on the value of the reduced interaction potential well depth, $\hat{\varepsilon}$, and in fact $\hat{\varepsilon} > 2$ is a necessary condition for significant aggregation to occur. Hence, for sufficiently small values of $\hat{\varepsilon}$ corresponding to high temperatures or shallow interaction potential well

Table 3.5 Simulation parameters used to produce Figure 3.7. Particle interactions were modeled using Lennard-Jones potentials and simulations were carried out using in-house BD code.

Parameter	Description	Value
N_p	Number of Particles	10000
f_v	Particle Volume Fraction	0.005
σ	Particle Diameter	3.4×10^{-10} m.
T	Temperature	121 K
$\frac{\sigma\gamma}{\sigma_{v_\infty}}$	Dimensionless Friction Coefficient	1.31

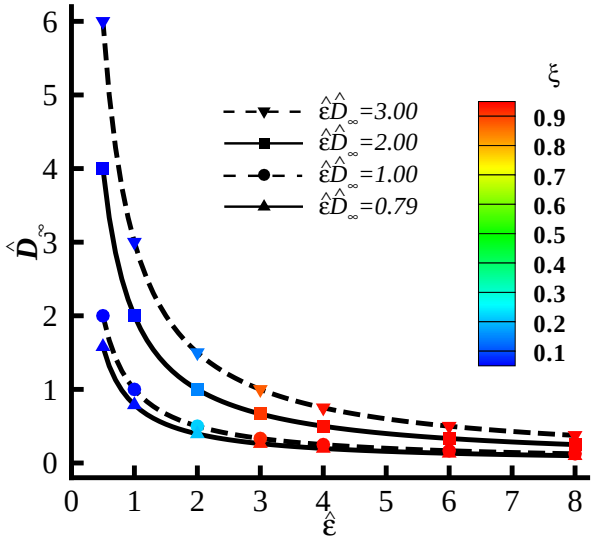

Figure 3.7 Clustering index (see color legend) as a function of reduced interaction potential well depth, $\hat{\varepsilon}$ and reduced diffusivity, $\hat{D}_\infty$. Each curve represents constant $\hat{\varepsilon}\hat{D}_\infty$. The region bounded by $\hat{\varepsilon}\hat{D}_\infty \ll 1$ represents the regime of validity of the position and velocity Langevin to PL reduction.

depths, colliding particles have a low probability of sticking because thermal fluctuations are large enough for the particles to overcome the potential energy barrier that otherwise would keep them together. Therefore $\hat{\varepsilon}$ controls how "sticky" the particles are and it must play a major role in the aggregation process. In contrast, ξ is relatively insensitive to the value of the reduced diffusivity. This latter observation is consistent with the fact that the Gibbs stationary solution of the Fokker-Planck equation corresponding to Eqs. 3.1 and 3.2 yields a Boltzmann distribution of particle coordinates independent of diffusivity [40].

3.4 Convergence of Brownian Dynamics Simulations

The convergence of Brownian dynamics simulations can be established by analyzing errors which occur when solving Eqs. 3.1 and 3.2 numerically. There are two main errors for numerical simulations of aggregation of colloidal nanoparticles (the round off error is not taken into account because it is not significant when simulating with double precision): one is the error which is related to the computational time step Δt and has a deterministic nature, when the other error is related to the number of independent simulations and has a statistical nature.

To establish convergence of BD simulations, a numerical test for the problem with known analytical solution is performed. From this test the computational time step Δt and the number of multiple independent simulations (MIS) required for accurate solution are determined. For this purpose a simple one-dimensional system of a single particle under the influence of a ramp-well potential is used. In this case the Langevin equations Eqs. 3.1 and 3.2 have the form

$$\begin{aligned} dx &= v_x dt \\ dv_x &= -\gamma v_x dt + \frac{F(x)}{m} dt + \Sigma_v dW \end{aligned} \tag{3.24}$$

The ramp-well potential is defined as

$$U(x) = \begin{cases} \infty, & 0 < x < \sigma \\ -\varepsilon \dfrac{x - x_a}{\sigma - x_a}, & \sigma \le x \le x_a \\ \infty, & x > L \end{cases} \tag{3.25}$$

where $(x_a - \sigma)$ is the width of the well, and x_a is related to the cut-off distance as shown in Figure 3.8. For such potential, if $x < x_a$ then the particle is considered to be in a *trapped* state, which corresponds to the case when a particle belongs to a cluster.

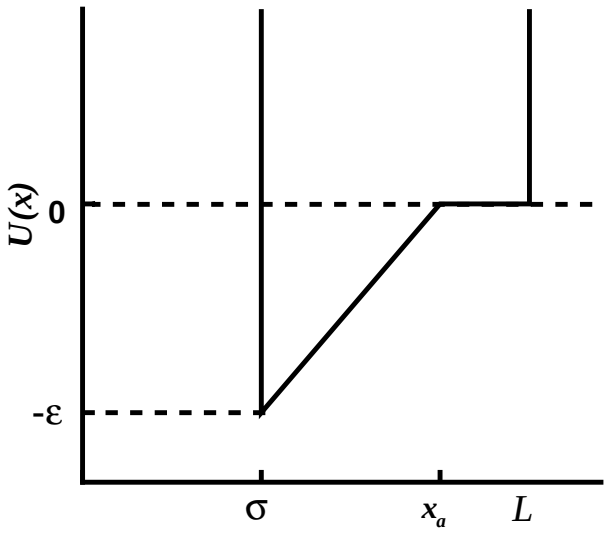

Figure 3.8 Representation of the ramp well potential.

Klyatskin [40] has shown that for the Hamiltonian system with a linear friction term (Eqs. 3.1 and 3.2) a steady-state probability distribution exists. In the one-dimensional case, the corresponding steady-state probability distribution has the form

$$P(x, v_x) = C_x P(x) C_{v_x} P(v_x), \tag{3.26}$$

where

$$P(x) = C_x \exp\left\{-\frac{2\gamma}{m\Sigma_v^2} U(x)\right\} \tag{3.27}$$

$$P(v_x) = C_{v_x} \exp\left\{-\frac{2\gamma}{m\Sigma_v^2} K(v_x)\right\} \tag{3.28}$$

where $U(x)$ is the potential energy, and $K(v_x)$ is the kinetic energy.

Constants C_x and C_{v_x} are found by integrating these equations over all values of x and v_x and equaling those integrals to one, thus

$$\begin{aligned} C_{v_x} &= \sqrt{\frac{\gamma}{\pi}}\frac{1}{\Sigma_v} \\ C_x &= \left[\frac{\Sigma_v^2 m(\sigma - x_a)}{2\gamma\varepsilon}\left(1 - \exp\left\{\frac{2\gamma\varepsilon}{\Sigma_v^2 m}\right\}\right) + (L - x_a)\right]^{-1} \end{aligned} \tag{3.29}$$

From the above equations it can be shown that the probability of the particle to lie in the interval $\sigma < x < x_a$ is equal to

$$p_a = p(\sigma < x \leq x_a) = \frac{1 - \exp\left\{\frac{2\gamma\varepsilon}{\Sigma_v^2 m}\right\}}{1 - \exp\left\{\frac{2\gamma\varepsilon}{\Sigma_v^2 m}\right\} + \frac{2\gamma\varepsilon(L - x_a)}{\Sigma_v^2 m(\sigma - x_a)}} \tag{3.30}$$

After analytical definition of the PDF solution, a set of numerical tests was then performed to identify the dependence of error on computational time step Δt and MIS number. For this purpose the system with such parameters is setting up: $\sigma = 1$, $m = 1$, $\varepsilon = 1$, $\gamma = 1$, $(x_a - \sigma) = 1$, $(L - x_a) = 0.6$, and $\sigma_{v_\infty}^2 = 1$. This set of parameters yelds the analytical value for the probability for particle to be in the trapped state as $p_a = 0.741$.

As it was discussed above, at least two sources of error are represented in the current test. One is the deterministic error D_p which occurs due to the presence of the finite time step Δt when integrating Langevin equations. Statistical error S_p occurs due to the fact that a finite number of the multiple independent simulations (MIS) can be computed. Thus, the total error is calculated as

$$e = \{p\}_{\Delta t,M} - p_a = (\{p\}_{\Delta t,M} - \langle p\rangle_{\Delta t,\infty}) + (\langle p\rangle_{\Delta t,\infty} - p_a) = S_p + D_p \tag{3.31}$$

where $\{p\}_{\Delta t,M}$ is the ensemble average for M independent simulations at computational timestep Δt, p_a is the analytical value of being in trapped state, and $\langle p\rangle_{\Delta t,\infty}$ is the expected value of the trapping probability for an infinite MIS at given computational time step Δt. In this expression, statistical error is defined as

$$S_p = \{p\}_{\Delta t,M} - \langle p\rangle_{\Delta t,\infty}, \tag{3.32}$$

and the deterministic error is defined as

$$D_p = \langle p\rangle_{\Delta t,\infty} - p_a. \tag{3.33}$$

In Eqs. 3.32 and 3.33 the value $\langle p \rangle_{\Delta t,\infty}$ is not defined and it needs to be estimated. In the present test, $\langle p \rangle_{\Delta t,\infty}$ is estimated by taking $M = 1 \times 10^7$ for different values of computational time step Δt.

It is expected that the deterministic error scales linearly with Δt as $D_p \sim \Delta t$. This dependence is expected because the deterministic error is defined as a difference of the first moments of p, and this scaling is expected for weak convergence [41]. This prediction was verified by computing deterministic error at different Δt values and by plotting D_p versus Δt (Figure 3.9). Also it was found that to keep D_p below 0.001, the computational time step should be $\Delta \hat{t} < 0.004$, where $\hat{t} = t\sigma_{v_\infty}/\sigma$. The statistical error S_p depends on the number of independent simulations M as $S_p \sim M^{-0.5}$. Figure 3.10 represents a dependence of the statistical error on M, which completely verifies analytical expectations. From this figure, by extrapolating to the value of $M = 1$, the statistical error for a single independent simulation is found to be equal up to 30%. Also at least 100 independent simulations are needed in order to reduce statistical error to the range of deterministic error D_p.

The main conclusions from the convergence of BD simulation tests are

i. The convergence test for a single particle in the ramp-well potential defines values for the computational time step $\Delta \hat{t} < 0.004$ and the number of multiple independent simulations $M > 100$ in order to keep values of statistical and deterministic errors below 0.1% for such a simple system.

ii. Computational results reproduce analytically predicted behavior for probability and the scaling of statistical and deterministic errors which verifies that implementation of BD is correct.

iii. Since the convergence test is done for a single particle, the number of simulations required to reach the same level of errors for the system of many nanoparticles which are involved in the aggregation process can be very large due to the large number of possible states for such a system. In this case other methods should be used which will reduce the statistical error more rapidly.

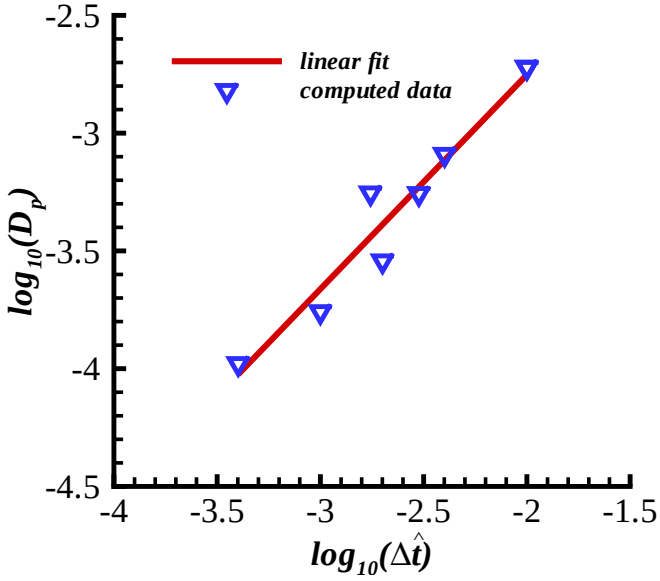

Figure 3.9 Deterministic error D_p versus computational time step. The slope of the linear fit is 0.96.

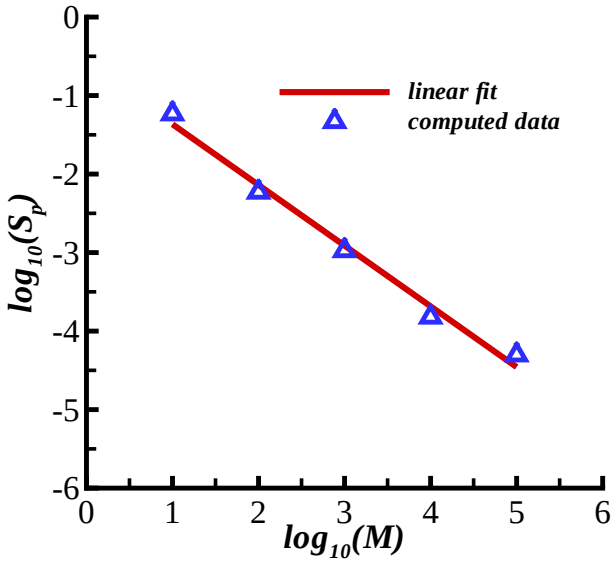

Figure 3.10 Statistical error S_p versus number of independent simulations at computational time step $\Delta\hat{t} = 0.002$. The slope of the linear fit is -0.54.

CHAPTER 4. RESULTS FROM THE SIMULATION OF AGGREGATIVE SYSTEMS

Although the Brownian dynamics method has been used by many investigators to simulate aggregation processes, little consideration has been given to the accuracy of such simulations even if statistically converged results can be obtained. Here the word "accuracy" is used in reference to how well the BD simulation predictions of aggregation reproduce those obtained from corresponding MD simulations, since the BD technique is essentially a reduction of the MD method. Because this reduction is obtained by eliminating the explicit representation of solvent molecules and replacing nanoparticle-solvent interactions with a mathematical model consisting of a stochastic fluctuating force and a deterministic frictional term, any discrepancies between predictions of the two methods are likely due to breakdowns in the assumptions and approximations implicit in these terms.

4.1 Comparison of Aggregation Statistics for MD and BD Simulations

The accuracy of BD simulations for dilute non-aggregating systems has previously been considered by Giro *et al.* [28]. These investigators considered the situation in which the nanoparticles are identical to the solvent molecules, and they showed that the BD simulations closely reproduce the equilibrium nanoparticle-nanoparticle radial distribution function, $g(r)$. However, they also found that the BD-computed nanoparticle diffusivities are larger than those predicted by the MD method, and they attributed this discrepancy to the fact that the frictional coefficient γ in the Langevin equation 3.2 is assumed to be constant, whereas a more realistic description (particularly for liquids) requires that the frictional coefficient be replaced by a time-dependent memory function. The fact that the BD method can accurately

compute the equilibrium nanoparticle-nanoparticle radial distribution function and yet incur noticeable error in the calculation of diffusivity is perhaps to be expected for reasons mentioned in the previous chapter - namely that the stationary solution of the Fokker-Planck equation is independent of the diffusivity. Hence, one expects that in general, BD predictions of system dynamics will not match the predictions of corresponding MD simulations, but that equilibrium quantities can be well-predicted by BD simulations. If follows, therefore, those BD simulations of the early stages of an aggregation process far from equilibrium may differ substantially from corresponding MD calculations. In spite of this observation (and the fact that MD simulation of systems with large aggregate-solvent size scale separation is not feasible), MD simulations with no size separation of nanoparticles and solvent particles are performed.

For such a test for MD simulations, a system of nanoparticles and solvent particles interacting by Lennard-Jones potential is chosen. The nanoparticle-nanoparticle interaction potential well depth, ε, was chosen such that nanoparticle aggregation was favored (as was discussed in the previous chapter). Additionally, the ratio of the mass of a single nanoparticle to a solvent molecule, $m_{solute}/m_{solvent} = 50$, is chosen to be relatively large to ensure that the nanoparticles has lower mobility than the solvent molecules, despite the fact that they have equal size. All MD simulations are carried out using the LAMMPS [26] software package on an IBM eServer Blue Gene which consists of 1024 dual-core PPC440 CPUs running at 700Mhz, with 512MB of RAM per node. Each run on the Blue Gene take up to 5 hours on 1024 CPUs. Other simulation details are listed in Table 4.1. In the case of BD simulations, the position and velocity equations are used because the position-only reduction is not applicable for this set of parameters.

In order to determine the accuracy of the BD simulations for aggregating systems, in Fig. 4.1 the extent of aggregation ξ is compared (as defined in 3.23) with that obtained from MD simulations for the system described in Table 4.1 for $\hat{\varepsilon} = 8$. It is clear that on the basis of the dimensionless time used to compare the two methods, the BD calculation predicts significantly more aggregation than does the MD simulation. Hence, in order to provide a better basis of comparison for the two methods, the predicted cluster size distributions at the

Table 4.1 Simulation parameters used to produce Figure 5.6. Particle interactions are modeled using Lennard-Jones potential. MD simulations are carried out using the LAMMPS [26] software package, BD simulations are carried out with in-house code.

Parameter	Description	Value (MD)	Value (BD)
$N_{solvent}$	Number of Solvent Particles	809,787	N/A
N_p	Number of Nanoparticles	10,000	10,000
$\varepsilon/k_B T_\infty$	Reduced Well Depth	4/8	4/8
$f_{v,solvent}$	Solvent Volume Fraction	0.44	N/A
$f_{v,nanop}$	Nanoparticle Volume Fraction	0.005	0.005
σ	Particle Diameter	3.4×10^{-10} m.	3.4×10^{-10} m.
$D_\infty/\sigma\sigma_{v_\infty}$	Dimensionless Diffusion Coefficient	N/A	0.262
$\sigma t_{stop}/\sigma_{v_\infty}$	Dimensionless Simulation Time	329.8	329.8

same extent of aggregation, ξ is compared for $\hat{\varepsilon} = 8$. This approach is applied in case

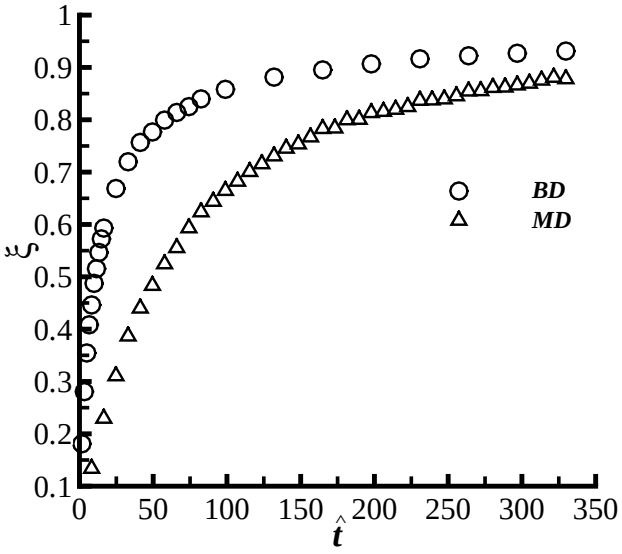

Figure 4.1 Extent of aggregation as a function of dimensionless time, $\hat{t} = \sigma t/\sigma_{v_\infty}$, for BD and MD simulations described in Table 4.1 for $\hat{\varepsilon} = 8$.

when the radial distribution functions are similar for the longest simulation time (Figure 4.2a) and is not applied for the case when the $g(r)$ values are significantly different (Figure 4.2b). Results for the radial distribution function, represented in Figure 4.2 clearly identify different regimes of aggregation process for MD simulations at different values of reduced well depth $\hat{\varepsilon}$. When $\hat{\varepsilon}$ is high (which is related to the higher probability of two nanoparticles to stick), a diffusion-limited aggregation is dominant. However, with smaller $\hat{\varepsilon}$, stickiness probability decreases to the level that a reaction-limited aggregation becomes dominant. Thus, in MD by varying value of the $\hat{\varepsilon}$, a different aggregation processes can be observed.

Figure 4.3a shows a direct comparison of the cluster size distributions computed using corresponding MD and BD simulations at $\xi = 0.89$ and $\hat{\varepsilon} = 8$. The agreement between the MD and BD simulations is very poor for the monomer frequency (471 monomers in the MD simulation and only 97 in the BD simulation); however the BD simulations predict a similar number average cluster size (8.3 particles/cluster versus 8.5 particles/cluster for MD). If the

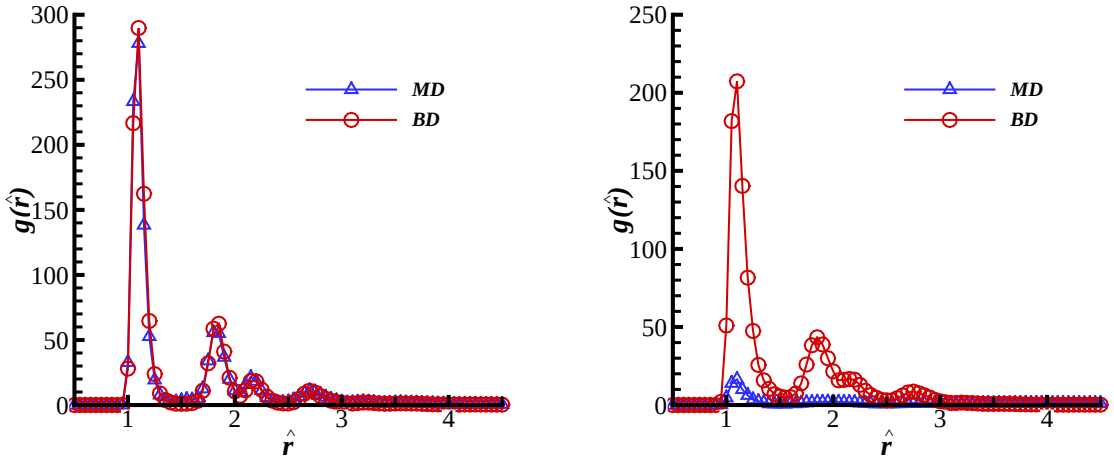

Figure 4.2 Comparison of the $g(\hat{r})$ from MD and BD simulations: a) simulations are done with $\hat{\varepsilon} = 8$, data is represented at time $\hat{t} = 329.8$; b) simulations are done with $\hat{\varepsilon} = 4$, data is represented at time $\hat{t} = 329.8$.

monomers are de-emphasized by computing the mass-average cluster size (ratio of the second to first moment of the cluster size distribution), the mean particle size is 20.2 particles/cluster for the MD simulations and 12.3 for BD simulations. The larger mass-average particle size in the MD simulations (despite the fact that the MD simulations produce a much larger population of monomers) is a reflection of the fact that the tail of the cluster size distribution (at the large size) for the MD case decays more slowly than in the BD case. For $\hat{\varepsilon} = 4$ there is no agreement for the cluster size distributions between MD and BD (Figure 4.3b) which is expected due to a significant difference in their radial distribution functions (Figure 4.2b). Further analysis of the case with $\hat{\varepsilon} = 4$ is not performed due to the significantly large difference in aggregation statistics for MD and BD.

An alternative method for comparing the cluster size distributions computed using the MD and BD simulation methods is to employ a dynamic scaling relation (see Appendix B for the definition of a CSD). In particular, it has been observed for a very wide range of aggregation processes that cluster size distributions can be collapsed by employing the following scaling

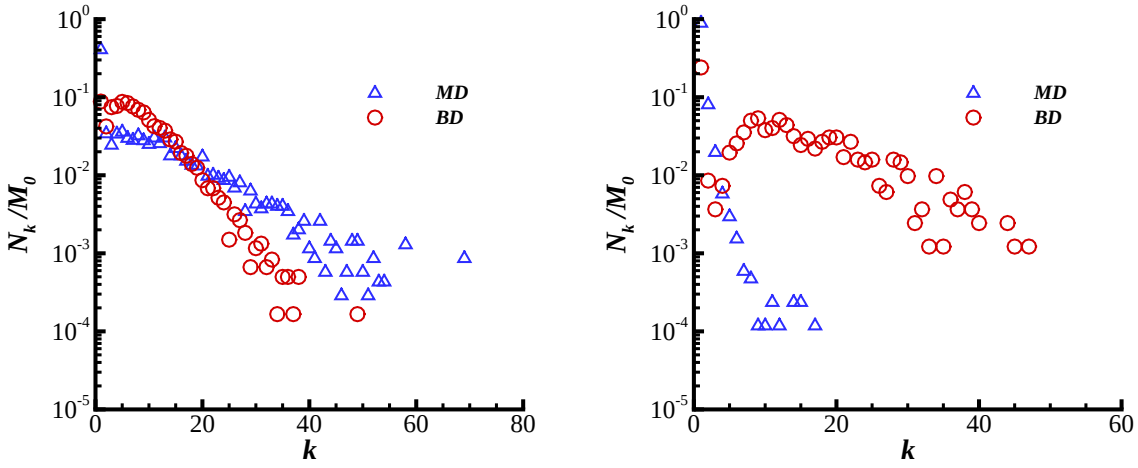

Figure 4.3 Comparison of cluster size distributions obtained from MD and BD simulations: a) simulations are done with $\hat{\varepsilon} = 8$, at the same extent of aggregation $\xi = 0.89$; b) simulations are done with $\hat{\varepsilon} = 4$, data is represented at time $\hat{t} = 329.8$.

parameter [42]:

$$N_k = s^{-2}(t)\phi(k/s(t)), \tag{4.1}$$

where N_k is the concentration of clusters containing k monomers, $s(t)$ is the mass-averaged particle size, and ϕ is a scaling function. If Eq. 4.1 is valid, then a plot of $s^2 N_k$ vs. k/s should collapse the cluster size distributions for all sufficiently large values of t such that the self-preserving regime has been reached. Figures 4.4 and 4.5 show such plots for the MD and BD cases, respectively for $\hat{\varepsilon} = 8$. Despite the relatively large statistical error associated with only carrying out a small number of independent simulations, in both cases the cluster size distributions do appear to fall on universal curves when plotted using Eq. 4.1. However, comparison of Figures 4.4 and 4.5 demonstrates that the shape of the scaling functions

are clearly different for the MD and BD cases. Consequently, it can be concluded that the BD simulations produce different cluster size distributions than the MD simulations, independent of any difficulties in comparing them due to a lack of information concerning the proper time scaling to be used. In particular, we see that the MD simulations generate cluster size

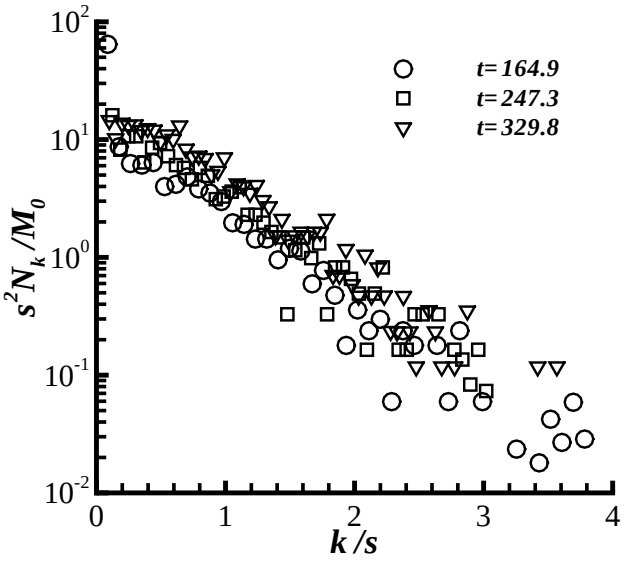

Figure 4.4 Scaled cluster size distributions for MD simulations at $\hat{\varepsilon} = 8$.

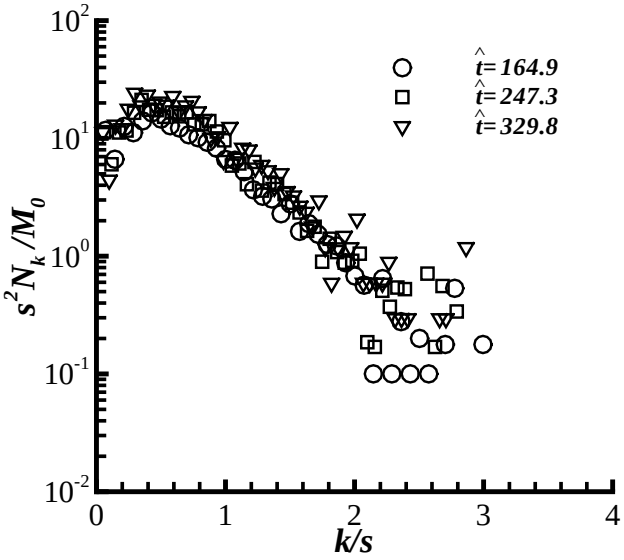

Figure 4.5 Scaled cluster size distributions for BD simulations at $\hat{\varepsilon} = 8$.

distributions that decay monotonically in size, whereas the BD simulations produce cluster size distributions that exhibit a maxima in N_k.

The morphology of the aggregates generated by MD and BD simulations can be compared by computing the volume fractal dimension, D_f. The volume fractal dimension can be related with the number of nanoparticles in cluster N_{cl}, the average size of the cluster (called the radius of gyration R_g), and the nanoparticle radius a as following [3, 5]

$$N_p = k_0 \left(\frac{R_g}{a} \right)^{D_f} \tag{4.2}$$

where k_0 is a prefactor of order unity. According to this expression, by plotting $\log(N_p)$ versus $\log(R_g)$ and by interpolating it with linear function, the slope of the obtained line must be D_f. The radius of gyration is calculated as [3]

$$R_g^2 = \frac{1}{N_{cl}} \sum_i (\mathbf{r}_i - \mathbf{r}_{cm})^2 \tag{4.3}$$

where $\mathbf{r}_i$ is the position of a i-th particle in a cluster, and $\mathbf{r}_{cm}$ is the position of the center of mass of a cluster. Figures 4.6 and 4.7 illustrate the results of the volume fractal dimension calculation for MD and BD simulations at $\xi = 0.89$ and $\hat{\varepsilon} = 8$. Both types of simulations produce clusters with $D_f \approx 2.5$ for MD, and $D_f \approx 2.0$ for BD which are relatively large values indicating that the clusters are quite compact. Indeed, this fractal dimension is comparable to the value produced in processes with diffusion-limited growth by monomer addition [8]. Hence one could infer that the collisions between small clusters and large clusters are more important than are the collisions between two large clusters in both the MD and BD simulations, even at large extents of aggregation. The structure of the clusters can be also analyzed with the powerful tool of light scattering analysis.

4.2 Light Scattering Analysis

Light scattering analysis (LS) is proposed as a direct method for investigation of aggregate structure [3, 5, 6, 43]. This method allows measurement of D_f even for a single cluster. In addition, the light scattering technique gives cluster structure information for the wide range of scales: from monomer size to the geometric size of a cluster. This feature provides for

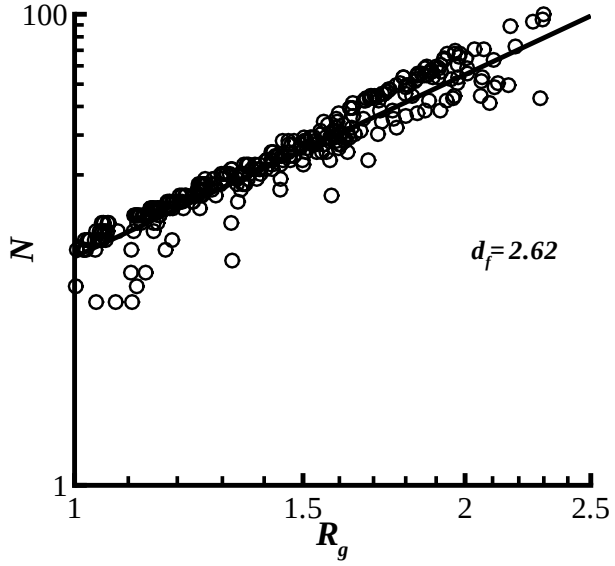

Figure 4.6 Number of monomers as a function of radius of gyration, R_g for MD simulations described in Table 4.1 at $\hat{\varepsilon} = 8$. The slope of the linear fit is the volume fractal dimension, D_f.

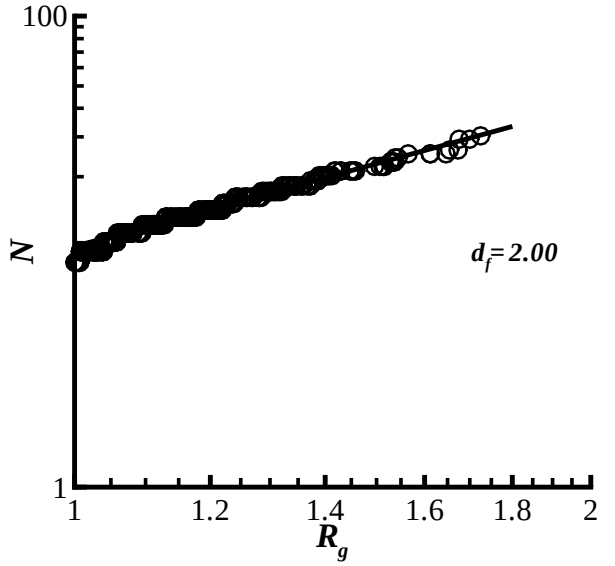

Figure 4.7 Number of monomers as a function of radius of gyration, R_g for BD simulations described in Table 4.1 at $\hat{\varepsilon} = 8$. The slope of the linear fit is the volume fractal dimension, D_f.

the discovery of any possible structure changes at different length scales, especially for the relatively large clusters. This gives the most complete description of the aggregate structure.

For the system of N nanoparticles, the intensity of elastically scattered light can be represented as

$$I(\mathbf{q}) = NF(\mathbf{q})S(\mathbf{q}) \tag{4.4}$$

where $\mathbf{q}$ is the scattering wave vector, which is defined as

$$q = |\mathbf{q}| = \frac{4\pi}{\lambda_l} sin(\theta/2) \tag{4.5}$$

where θ is the scattering angle, λ_l is the wavelength of light, $S(\mathbf{q})$ is the static structure factor, where

$$S(\mathbf{q}) = \frac{1}{N} \sum_{k}^{N} \sum_{l}^{N} exp[i\mathbf{q} \cdot (\mathbf{r}_k - \mathbf{r}_l)] \tag{4.6}$$

Due to a spherical shape of nanoparticles with uniform density, Eq. 4.6 can be reduced to

$$S(\mathbf{q}) = \frac{1}{N} \left| \sum_{k}^{N} exp[i\mathbf{q} \cdot \mathbf{r}_k] \right|^2 = \frac{1}{N} \left| \sum_{k}^{N} [cos(\mathbf{q} \cdot \mathbf{r}_k) + i\ sin(\mathbf{q} \cdot \mathbf{r}_k))] \right|^2 \tag{4.7}$$

and $F(\mathbf{q}) \rightarrow F(q)$ is the form factor for a sphere,

$$F(q) = \left[3 \frac{sin(qa) - qa\ cos(qa)}{(qa)^3} \right]^2 \tag{4.8}$$

Because all modeled systems are isotropic in cluster position and orientation it is valid to perform a spherical averaging by selecting over 200 different $\mathbf{q}$ values of constant magnitude, so $S(\mathbf{q}) \rightarrow S(q)$. This was done by creating the set of angles (θ, ϕ) according to a uniform differential solid angle $d\Omega$, and q is calculated from:

$$\mathbf{q} = |\mathbf{q}|(sin(\theta)cos(\phi)\mathbf{e}_1 + sin(\theta)sin(\phi)\mathbf{e}_2 + cos(\theta)\mathbf{e}_3) \tag{4.9}$$

where $\mathbf{e}_i$ is the i-th Cartesian unit vector.

In case of a self-similar fractal aggregate with a fractal dimension D_f, $I(q)$ has the following three regimes: the first regime is for small values of q (the so-called Rayleigh regime), where $I(q) = N$ the number of monomers per cluster. The second regime is for intermediate values

of q, where $I(q) \sim q^{-D_f}$. The third regime is for very large q when Porod's law can be applied, so $I(q) \sim q^{-4}$ [4].

To validate the in-house LS code, a system of 100,000 nanoparticles where distributed in a 3-d square lattice with period $d_l = 2$. Positions of the light scattering peaks in the crystal lattice must be distributed according to Bragg's law

$$2d_l \sin(\theta/2) = n\lambda_l \tag{4.10}$$

where λ_l is the wavelength of an incident light, n is the integer corresponding to the order of intensity peak, and θ is the angle between incident light and the scattering panels. The value for the wavelength is chosen arbitrarily to be $\lambda_l = 0.251$.

Table 4.2 Validation of LS code

n	1	2	3	4
θ (Bragg's law)	7.201	14.431	21.719	29.097
θ (LS code)	7.197	14.435	21.719	29.094

For such a system, an LS analysis is performed and correspondent positions of peaks are computed and compared with analytically expected ones(Table 4.2). The excellent match of computational data with analytical values verifies the LS code and allows us to use it for systems with unknown structures.

In BD (as well as in MD) the conservative force is not calculated for all the possible pair separations between nanoparticles. Instead, such parameter as a cut-off distance r_c is introduced. In this way, force is calculated for the particles separated by a cut-off distance or smaller. All other separations do not influence the force calculations. This approach significantly decreases simulation time without interfering with computational accuracy. Such an approach is applicable for a monotonically decaying interaction potential which is very close to zero value at $r > r_c$. Therefore, it would be interesting to see how LS results depend on the r_c value. For

this purpose BD simulations of the aggregation of colloid nanoparticles which interact through the Lennard-Jones potential were performed for $r_c = 2.5\sigma = 5a$ and $r_c = 1.5\sigma = 3a$, where a is the nanopartile radius. All the parameters for these simulations are described in Table 4.3. Figure 4.8 represents LS analysis of the largest clusters obtained from these BD simulations. The largest clusters consist of $N = 8,900$ and $N = 8,717$ nanoparticles for $r_c = 3a$ and $r_c = 5a$

Table 4.3 Simulation parameters used to produce Figure 4.8. Particle interactions are modeled using Lennard-Jones potentials.

Parameter	Description	Value
N_p	Number of Nanoparticles	108,882
ε/k_BT_∞	Reduced Well Depth	4
$f_{v,nanop}$	Solute Volume Fraction	0.035
σ	Particle Diameter	3.4×10^{-10} m.
$D_\infty/\sigma\sigma_{v_\infty}$	Dimensionless Diffusion Coefficient	0.524
$\sigma t_{stop}/\sigma_{v_\infty}$	Dimensionless Simulation Time	32.98
$\sigma\Delta t/\sigma_{v_\infty}$	Dimensionless Computational Time Step	0.0025

correspondingly. The positions of cut-off distances are marked by a dashed line and labeled correspondently. According to the previous work [5], in the interval $a/R_{g,G} < qa < 2$ structure factor $S(q)$ should be $\sim q^{-D_f}$, where $D_f = 1.78$ is the fractal dimension, and $R_{g,G}$ is the ideal gel point radius of gyration, and its defined as

$$R_{g,G} = a\left[k_0^{-1}\left(\frac{D_f+2}{D_f}\right)^{d/2}\alpha\right]^{1/(D_f-d)} \tag{4.11}$$

where $k_0 \simeq 1.3$, d is the space dimension, and α is the nanoparticle volume fraction. However, in this case $D_f \simeq 3$ for the range $(a/r_c < qa < 2)$ for both cut-off distances. Such behavior can be explained that by implementing Lennard-Jones potential into BD, the structure of

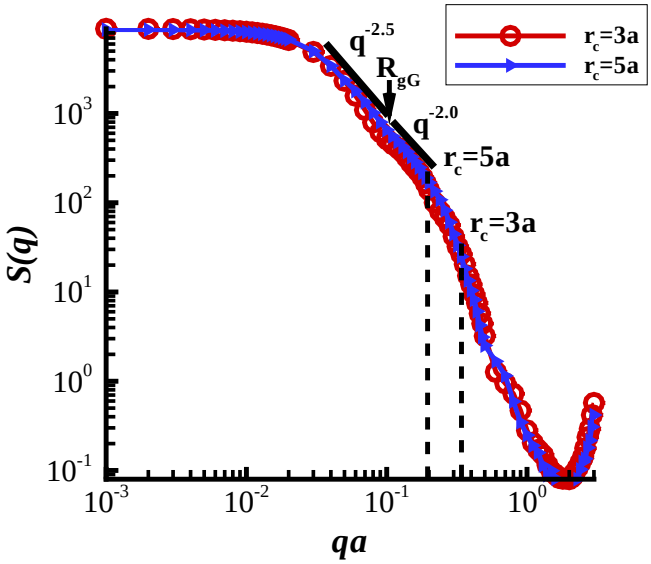

Figure 4.8 Structure of the largest cluster for 3-D BD simulation with implemented LJ potential for $r_c = 5.0a$ and $r_c = 3.0a$

the aggregate cannot be described correctly for the scale of a potential's range. At the same time, by setting up the cut-off distance $r_c \to \infty$ the LS results should be similar to those obtained for $r_c = 5a$, because for LJ potential as $r > 5a$, the interaction potential $U \to 0$. Thus, the only part of the LS curve with $qa < a/r_c$ can be taken into account for further analysis. In the LS plot there are two ranges for qa that can be clearly defined. In the range $(R_{g,G} < qa < a/r_c)$, results are similar with the well-known results for DCLA where $D_f \sim 1.8$, when for $(qa < R_{g,G})$ the results are close to the DLA, where $D_f \sim 2.5$ [4]. However, it is hard to make a final decision about fractal dimension values because of a very short dynamic range where D_f can be measured. An increase of dynamic range can be reached in a different ways. The first is to decrease the cut-off distance r_c. In this case, the dynamic range will increase, however the simulation accuracy reduces significantly due to a loss of accuracy during force calculations (even LS results look similar for both values of r_c in Figure 4.8). Therefore, the first approach cannot be accepted. The second way is to shift the ideal gel point radius of gyration to the left. This can be done by decreasing the nanoparticle volume fraction. However, the aggregation process takes longer for systems with a lower volume fraction. Moreover, the

number of nanoparticles in the system should be increased to maintain a high possibility of large cluster formation. For example, by reducing the nanoparticle volume fraction to $\alpha = 0.015$, and increasing the number of nanoparticles in a system to $N = 500,000$, the computational time for BD simulation would be 50-70 hours on a single processor in order to obtain the maximum cluster containing up to $50,000$ nanoparticles. For even larger systems, a single processor BD simulation cannot be done in a reasonable computational time and some additional steps to speed up BD calculations are required. Thus, to speed up BD simulations the BD code must be parallelized.

CHAPTER 5. IMPROVED MODELING OF AGGREGATING SYSTEMS

When aggregation occurs in the system of colloidal nanoparticles with no external forces, the dynamics of such an aggregation process is usually controlled by several statistics. The first statistic is the self-diffusion coefficient of nanoparticles, which defines how fast two nanoparticles can reach each other to form a cluster. A second important statistic is the surface chemistry of the nanoparticles which controls the nanoparticle stickiness. This statistic corresponds to the attractive part of the interaction potential and potential well depth $\hat{\varepsilon}$ for a model system. This second parameter controls the aggregation regime (diffusion-limited aggregation vs. reaction-limited aggregation).

Analysis of only these statistics will be sufficient to simulate aggregation of colloidal nanoparticles with such models as DLA, RLA, *etc*, because in these models a nanoparticle or cluster (in case of DLCA, *etc.*) is introduced into the system and it diffuses and attaches to the steady cluster with stickiness probability p_{stick}. However, when modeling the dynamic of aggregation of colloidal nanoparticles with MD or BD approaches, considering only these two statistics may be not enough to describe the aggregation process in the correct way. This is true because in the case of dynamic aggregation, all of the nanoparticles and clusters are moving and the relative dispersion of pair diffusion (which is related to the pair correlation function) is the parameter which plays an important role and should be considered when describing the aggregation process.

Because the radial distribution function $g(r)$ describes only the pair separation statistic and does not describe any other aggregation statistics such as cluster size distribution *etc.*, it is questionable if $g(r)$ is a sufficient statistic to describe aggregating structures. To answer this

question it is important to answer another question: Is it possible to construct two different aggregating systems with the same cluster size distribution (CSD), but different $g(r)$? If the answer is negative, than $g(r)$ is a sufficient statistic to describe an aggregating structure, but if the answer is positive, the $g(r)$ is not a sufficient statistic. The answer to this question can be easily found by considering a system with an arbitrary distribution of cluster sizes. For such a system $g(r)$ can be computed. Then, let us rescale all the positions of nanoparticles in this clustering system by a factor of 0.98. In this case the distances between pairs of nanoparticles will slightly decrease but the CSD will not change at all. It is obvious that $g(r)$ for this new system will be different than for the original one because the size separation statistic is changed. Thus, if two systems have the same CSD they may have different $g(r)$. Therefore, the CSD statistic should be analyzed as well, because $g(r)$ is not sufficient but only necessary statistic for accurate description of an aggregating system.

In the context of accurately computing nanoparticle aggregation statistics, there is the need for BD to accurately reproduce the pair correlation function, in addition to the diffusion coefficient. This leads to the derivation of the evolution of the second-order density (unnormalized radial distribution function) corresponding to the MD and BD dynamical equations.

In the early work Giro *et al.* [28] have shown that for systems at equilibrium (with no aggregation occurs) the $g(r)$ from MD and BD simulations is significantly different if the same Lennard-Jones potential is implemented in both approaches. However, in case of the aggregation of colloidal nanoparticles, the $g(r)$ values for MD and BD simulations depend on the aggregation regime. As it was shown in the previous chapter, when aggregation occurs due to the DLA regime there is no significant difference in the $g(r)$ (Figure 4.2a) and there is no need for a second-order density analysis. At the same time, when aggregation occurs due to the RLA regime there is a significant difference in the $g(r)$ for MD and BD (Figure 4.2b). In this case a second-order density analysis can be used to match the $g(r)$ from MD and BD simulations.

5.1 Evolution of the Second-Order Density

Second order density is an important quantity when clustering systems are considered. Second-order density $\rho^{(2)}(\mathbf{x}_1, \mathbf{x}_2, \mathbf{v}_1, \mathbf{v}_2, t)$ is defined as [44]

$$\rho^{(2)}(\mathbf{x}_1, \mathbf{x}_2, \mathbf{v}_1, \mathbf{v}_2, t) = \langle f_1' f_2' \rangle \tag{5.1}$$

where $f_k' = \sum_{i=1}^{N} \delta(\mathbf{v}_k - \mathbf{V}^{(i)})\delta(\mathbf{x}_k - \mathbf{X}^{(i)})$, $\{\mathbf{X}^{(i)}, \mathbf{V}^{(i)}, i = 1, ...N\}$ are the position and velocity of the N nanoparticles in the ensemble, the product $\langle f_1' f_2' \rangle$ is formed over distinct pairs ($j \neq i$) over all realizations of the multiparticle system. The evolution of the second-order statistics $\rho^{(2)}$ is derived from Eq. 5.1, when the i-th particle evolves according to $d\mathbf{X}^{(i)}/dt = \mathbf{V}^{(i)}$, and $d\mathbf{V}^{(i)}/dt = \mathbf{A}^{(i)}$, where $\mathbf{A}^{(i)}$ is the acceleration experienced by the particle. Thus, after differentiation of Eq. 5.1 with additional assumptions of statistical homogeneity in both the position space as well as velocity space the following expression is obtained (see Appendix C for details) [45],

$$\frac{\partial \rho^{(2)}(\mathbf{r}, \mathbf{w}, t)}{\partial t} + \nabla_{\mathbf{r}} \cdot \left(\mathbf{w} \rho^{(2)} \right) + \nabla_{\mathbf{w}} \cdot \left(\langle \Delta \mathbf{A} | \mathbf{r}, \mathbf{w}, t \rangle \rho^{(2)} \right) = 0 \tag{5.2}$$

where $\mathbf{r} = \mathbf{x}_2 - \mathbf{x}_1$ is the relative separation, $\mathbf{w} = \mathbf{v}_2 - \mathbf{v}_1$ is the relative velocity, and $\langle \Delta A | \mathbf{r}, \mathbf{w}, t \rangle = \langle A^{(2)} | \mathbf{r}, \mathbf{w}, t \rangle - \langle A^{(1)} | \mathbf{r}, \mathbf{w}, t \rangle$ is the average relative acceleration. This quantity evolves by a transport equation that contains two terms: one is a transport term in the relative pair-separation space that contains the pair relative velocity, and the other is a transport term in the pair relative velocity space that contains the conditional expectation of pair relative acceleration.

Analogous equation for the evolution of the second-order density can be derived for Langevin equations 3.1 and 3.2. Thus, understanding the behavior of the pair relative velocity and pair relative acceleration terms for both the MD and BD approaches can provide insight into the development of coarse-grained potentials for BD. An average relative acceleration is the third order statistic, which involves arbitrary nanoparticles 1, 2, and probe particle p. Simultaneous statistical description of two pair separations ($|\mathbf{r}| = |\mathbf{x}_2 - \mathbf{x}_1|$, $|\mathbf{r}'| = |\mathbf{x}_1 - \mathbf{x}_p|$ for particle 1 and $|\mathbf{r}| = |\mathbf{x}_2 - \mathbf{x}_1|$, $|\mathbf{r}''| = |\mathbf{x}_2 - \mathbf{x}_p|$ for particle 2) is required.

The total average relative acceleration can be decomposed into two parts: direct relative acceleration $\langle \Delta A_d | \mathbf{r} \rangle$ and indirect relative acceleration $\langle \Delta A_i | \mathbf{r} \rangle$

$$\langle \Delta A | \mathbf{r} \rangle = \langle \Delta A_d | \mathbf{r} \rangle + \langle \Delta A_i | \mathbf{r} \rangle \tag{5.3}$$

Direct relative acceleration occurs due to the direct interaction of the nanoparticles 1 and 2, and indirect relative acceleration occurs due to the interaction of particle 1 with the probe particle p, and particle 2 with the probe particle p, excluding interaction between nanoparticles 1 and 2. It is convenient to make such a decomposition because an indirect average relative acceleration is the point of our interest, but in many cases its magnitude is lower than the magnitude of the direct average relative acceleration. Also, a direct average relative acceleration is independent of the radial distribution function $g(r)$, when an indirect average relative acceleration depends on the $g(r)$.

An average relative acceleration can be represented as follows, by assuming a pair-additive interaction between nanoparticles

$$\begin{aligned} &\langle \Delta \mathbf{A}^{(2)(1)}(\mathbf{r}', \mathbf{r}'') \rangle = \int \langle \Delta \mathbf{A} | \mathbf{r} \rangle \rho^{(2)}(\mathbf{r}) d\mathbf{r} = \\ &= \int \mathbf{A}^{(2)}(\mathbf{r}'', \mathbf{r}) \rho^{(3)}(\mathbf{r}'', \mathbf{r}) d\mathbf{r}'' d\mathbf{r} - \int \mathbf{A}^{(1)}(\mathbf{r}', \mathbf{r}) \rho^{(3)}(\mathbf{r}', \mathbf{r}) d\mathbf{r}' d\mathbf{r} \end{aligned} \tag{5.4}$$

A third-order density term $\rho^{(3)}$ is unknown. It is determined by applying $\rho^{(3)}(\mathbf{r}', \mathbf{r}) = \lambda^3 h(\mathbf{r}', \mathbf{r})$. This relation is defined by analogy with the definition of the second-order density term $\rho^{(2)}(\mathbf{r}) = \lambda^2 g(\mathbf{r})$, where λ is the number density of the particles for which an average relative acceleration is calculated. The third-order correlation function $h(\mathbf{r}', \mathbf{r})$ can be expressed in terms of the pair correlation function:

$$h(\mathbf{r}', \mathbf{r}) = h(\mathbf{r}' | \mathbf{r}) g(\mathbf{r}) \tag{5.5}$$

and therefore $\rho^{(3)}(\mathbf{r}'', \mathbf{r}) = \lambda h(\mathbf{r}'' | \mathbf{r}) \rho^{(2)}(\mathbf{r})$. By substituting all these expressions into Eq. 5.4 an expression for the average relative acceleration is

$$\langle \Delta \mathbf{A} | \mathbf{r} \rangle = \lambda \int \mathbf{A}^{(2)}(\mathbf{r}'', \mathbf{r}) h(\mathbf{r}'' | \mathbf{r}) d\mathbf{r}'' - \lambda \int \mathbf{A}^{(1)}(\mathbf{r}', \mathbf{r}) h(\mathbf{r}' | \mathbf{r}) d\mathbf{r}' \tag{5.6}$$

To verify a code for the average relative acceleration calculations, a simple test is constructed where computational and analytical data are compared.

5.2 Test Calculations

For the analytical calculations of the average relative acceleration, a static test with particles placed along the line (1-d case) and particles on the plane (2-d case) are considered. All the particles interact through the Lennard-Jones potential

$$U = 4\varepsilon \left(\left(\frac{\sigma}{r} \right)^{12} - \left(\frac{\sigma}{r} \right)^{6} \right) \tag{5.7}$$

where ε is the well depth of the potential, and σ is the particle diameter. Particles are distributed according to the Matérn process [47] with hard-core distance equal to the particle diameter (hard-core distance defines the minimum possible distance between two neighbor particles). This choice of system allows for use of an analytical expression for the acceleration and radial distribution function $g(r)$ (Figure 5.1), as well as giving a simpler expression for the

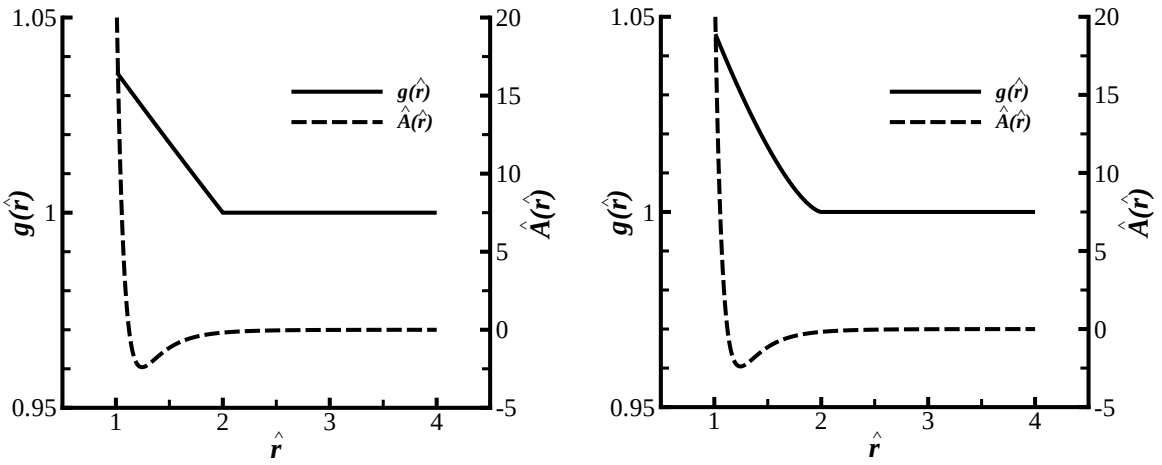

Figure 5.1 Analytical Matern $g(\hat{r})$ at $\hat{\lambda}_m = 0.1$ (left axis), and dimensionless acceleration (right axis): a) 1-d case, b) 2-d case.

integral for the relative acceleration calculation Eq. 5.6. Table 3.2 lists all the characteristic parameters which are used in the present study, where the acceleration is calculated from the Lennard-Jones potential U by the following expression

$$\mathbf{A}(\mathbf{r}) = \frac{\mathbf{F}(\mathbf{r})}{m} = -\frac{1}{m} \nabla_{\mathbf{r}} U \tag{5.8}$$

For a 1-d case, by calculating the expectation of an indirect relative acceleration between arbitrary particles 1 and 2 due to the presence of the probe nanoparticle p (interaction between particles 1 and 2 is excluded), Eq. 5.6 can be rewritten in a scalar form. To estimate the $h(\mathbf{r}|\mathbf{r})$ value, the following assumptions are applied

$$h(\mathbf{r}'|\mathbf{r}) \cong g(\mathbf{r}') \tag{5.9}$$

$$h(\mathbf{r}''|\mathbf{r}) \cong g(\mathbf{r}'') \tag{5.10}$$

and

$$\langle \Delta A|r\rangle \cong \lambda \int A(r'',r)g(r'')\mathbf{e}_{2p}\cdot\mathbf{e}_{21}dr'' - \lambda \int A(r',r)g(r')\mathbf{e}_{1p}\cdot\mathbf{e}_{21}dr' \tag{5.11}$$

where $\mathbf{e}_{21} = \mathbf{r}/|\mathbf{r}|$, $\mathbf{e}_{1p} = \mathbf{r}'/|\mathbf{r}'|$, and $\mathbf{e}_{2p} = \mathbf{r}''/|\mathbf{r}''|$ are the unit vectors.

Based on the relative positions of particles 1, 2, and p, scalar products in Eq. 5.11 will have different values. For a 1-d case there are three unique cases represented in Figure 5.2 which should be considered. In this figure, gray areas correspond to the prohibited values for the $\hat{r}'$ and $\hat{r}''$. In Case 1, p nanoparticle is placed between particles 1 and 2, so $\mathbf{e}_{2p}\cdot\mathbf{e}_{21} = 1$, and $\mathbf{e}_{1p}\cdot\mathbf{e}_{21} = -1$. In Case 2, p nanoparticle is placed on the left side from particles 1 and 2, thus $\mathbf{e}_{2p}\cdot\mathbf{e}_{21} = 1$, and $\mathbf{e}_{1p}\cdot\mathbf{e}_{21} = 1$. In Case 3, p nanoparticle is placed on the right side from particles 1 and 2, and $\mathbf{e}_{2p}\cdot\mathbf{e}_{21} = -1$, and $\mathbf{e}_{1p}\cdot\mathbf{e}_{21} = -1$. A schematic for Case 3 is not represented because the pattern will be exactly the same as in Case 2 but for the negative values of $\hat{r}'$ and $\hat{r}''$. After considering all these cases, the final expression for the average relative acceleration in the 1-d case is

$$\langle \Delta A|r\rangle \cong -2\int_{r-h}^{r+h} A(u)g(u)du \tag{5.12}$$

where $h = \sigma$ is the hard core distance, and σ is the particle diameter. Similar analysis is performed for a 2-d case which is much more complicated due to increasing of dimensionality. Analytical expression for a 3-d case is not considered due to dramatic complications during analytical integrations. The results of these analytical calculations for 1-d and 2-d cases are represented in Figure 5.3. Thus, after obtaining an analytical solution, an in-house code which is written to extract the average relative acceleration from the experimental data can be verified by simulating a set of simple tests.

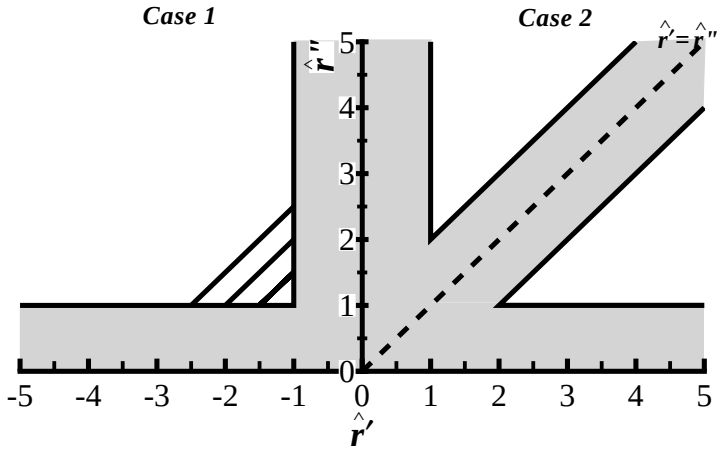

Figure 5.2 Schematic of all possible values of $\hat{r}'$ and $\hat{r}''$ in 1-d case with prohibited gray area.

In the first test, the indirect average relative acceleration of identical particles is computed. In this case 150,000 identical particles in the 1-d case and 823,000 identical particles in the 2-d case were generated according to the Matérn process with $h = \sigma$, and with reduced number density $\hat{\lambda}_m = 0.1$. Then, for each of $N(N-1)/2$ particle pair, separated by $\hat{r}$, the indirect relative acceleration on this pair due to all other $N-2$ particles is calculated (an interaction between particles in the pair is excluded). After this, obtained data are averaged over all pairs separated by the same distance $\hat{r}$. The results of these computations are represented in Figure 5.3. A good agreement between analytically calculated and computed data for $\hat{\lambda}_m = 0.1$ is observed even by taking into account that analytical data is not exact (Eq. 5.11) and obtained after applying crude approximation. Generally, a good matching of computational and analytical results is observed for $\hat{\lambda}_m \leq 0.1$, when for $\hat{\lambda}_m > 0.1$ the approximation represented in Eq. 5.11 does not hold.

In the 1-d case (Figure 5.3a) a negative value for the average relative acceleration at $1 < \hat{r} <$

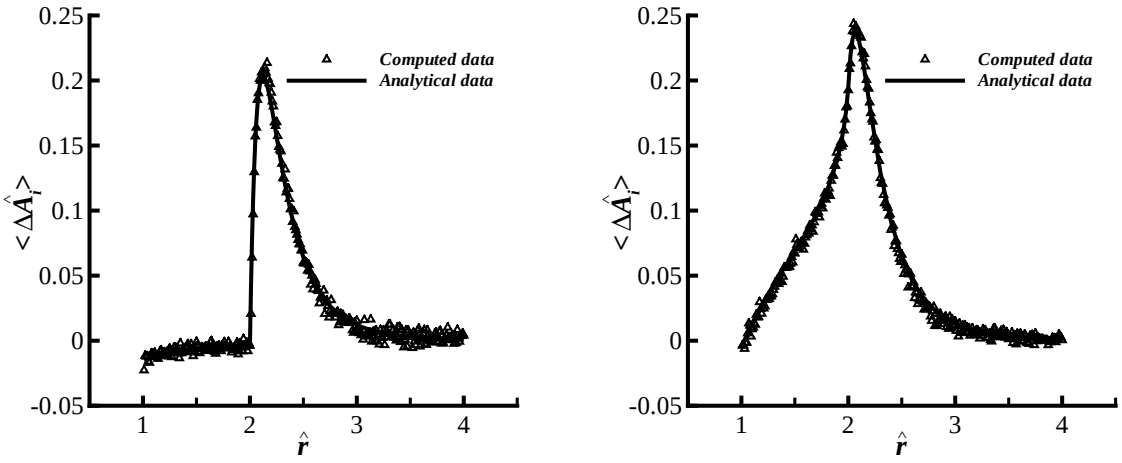

Figure 5.3 Indirect average relative acceleration (computed and analytically calculated) at $\hat{\lambda}_m = 0.1$: a) 1-d case, computed data is obtained for 150,000 identical particles and is averaged over 3,000 MIS, b) 2-d case, computed data is obtained for 823,000 identical particles and is averaged over 240 MIS.

2 is observed which corresponds to the attraction between the particles. Further, at $\hat{r} = 2.15$ a strong repulsion peak between particles is observed which is decaying to 0 at larger $\hat{r}$ values. This behavior can be explained by considering a geometrical place of test particles 1, 2, and probe particles p in 1-d. In this case when test particles are separated by $\hat{r} < 2$, probe particles p can be placed anywhere except between the test particles 1 and 2 (nanoparticle overlapping is prohibited). In this case, on average, probe particles p "pushes" the test particles from the left and right and as a result, test particles move toward each other. This corresponds to the nanoparticle attraction. However, when the distance between test nanoparticles is large enough to fit a probe particle between them ($\hat{r} \geq 2$), a strong repulsion occurs. And at large separation of the test particles, an acceleration of nanoparticle 1 and 2 due to p becomes close to 0 as $g(\hat{r}) = 1$ (Figure 5.1). These results confirm that an indirect average relative acceleration for the identical particles is computed correctly. However, in most real applications a mixture of at least two types of molecules is considered. Because of this, a second test for extraction of an indirect average relative acceleration from a mixture is conducted.

For this test, the same system as in the previous case is considered with only the difference that 29.5% of all the particles are called A-type particles (nanoparticles) and the rest of the particles are called B-type solvent molecules. The size and the mass of A-type and B-type particles is the same, but the well-depth of the pair interaction potential for $A-A$, $A-B$, and $B-B$ type interaction is different and is defined as $\hat{\varepsilon}_{AA}/\hat{\varepsilon}_{BB} = 8.0$ and according to Lorentz-Berthelot mixing rule $\hat{\varepsilon}_{AB} = (\hat{\varepsilon}_{AA} \cdot \hat{\varepsilon}_{BB})^{1/2} = \sqrt{8.0}$. An analytical expression for the average relative acceleration of $A-A$ particles due to both A-type and B-type particles can be derived from Eq. 5.6 by substituting

$$\mathbf{A}^{(1)}(\mathbf{r}', \mathbf{r}) = \mathbf{A}^{(1)}_{AA}(\mathbf{r}'', \mathbf{r}) + \mathbf{A}^{(1)}_{AB}(\mathbf{r}'', \mathbf{r}) \tag{5.13}$$
$$\mathbf{A}^{(2)}(\mathbf{r}'', \mathbf{r}) = \mathbf{A}^{(2)}_{AA}(\mathbf{r}'', \mathbf{r}) + \mathbf{A}^{(2)}_{AB}(\mathbf{r}'', \mathbf{r})$$

Computational data is obtained for 44,000 A-type particles and 106,000 B-type particles in the 1-d case and for 243,000 A-type particles and 580,000 B-type particles in the 2-d case. Then, the calculations are done in a similar manner as for the previous case, with the only difference that the relative acceleration between only A-type particles pairs due to the effect of both A-type and B-type particles is calculated. A comparison of analytical data and computationally extracted data represent good agreement (Figure 5.4) with the larger spreading of the computational data around analytical data than is observed in the previous case (Figure 5.3). This large spreading is caused by a significant reduction of the number of pairs which are involved in the relative acceleration computations.

Test runs for indirect average relative acceleration extractions validate an in-house code for the pure solvent system of identical particles as well as for the mixture of different types of particles. When the relative acceleration is extracted from the mixture of molecules, an additional number of independent simulations should be done to compensate loss of the precision. Good agreement between analytical calculations and computationally extracted data is observed for both 1-d and 2-d cases. This is a good sign that the same algorithm should work for a 3-d case as well. Direct comparison of analytical data with computational data in the 3-d case is not represented in this work because analytical calculations of the average relative acceleration for a 3-d case is a challenging task.

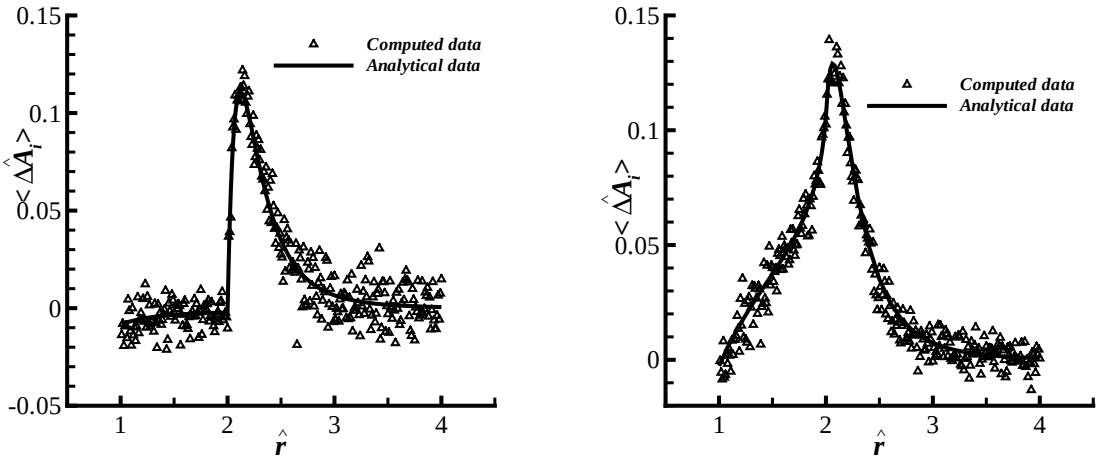

Figure 5.4 Indirect average relative acceleration (computed and analytically calculated) of A-type particles in a mixture with $\hat{\lambda}_{A+B} = 0.1$ and $\hat{\varepsilon}_{AA}/\hat{\varepsilon}_{BB} = 8.0$: a) 1-d case, computed data is obtained for 44,000 A-type particles and 106,000 B-type particles. Data is averaged over 3000 MIS, b) 2-d case, computed data is obtained for 243,000 A-type particles and 580,000 B–type particles. Data is averaged over 240 MIS.

5.3 Relative Acceleration in an Equilibrium System

Calculation of the relative acceleration for dynamic systems is the point of interest for the relative acceleration problem. One of the simplest 3-d systems is a system of identical non-aggregative particles at an equilibrium state. To generate such a system the MD simulation of a 3-d system of 823,218 identical particles with well depth of the Lennard-Jones potential $\hat{\varepsilon} = 1.0$ and the volume fraction $\alpha = 0.45$ is performed. Computation stops when the system reaches a steady state. In the present case $\hat{t}_{stop} = 5.94$ in σ/σ_{v_∞} units, where σ is the particle diameter, $\sigma^2_{v_\infty} = k_B T_\infty/m$ is the velocity variance, k_B is the Boltzmann coefficient, T_∞ is the reference temperature, and m is the particle mass. All MD simulations were carried out using LAMMPS [26] software package on an IBM eServer Blue Gene which consists of 1024 dual-core PPC440 CPUs running at 700Mhz, with 512MB of RAM per node.

Obtained from MD simulation data are post-processed and an indirect average relative

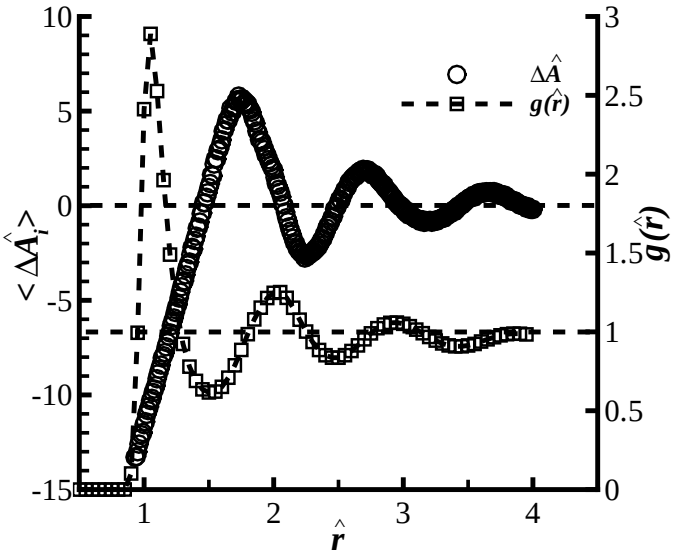

Figure 5.5 Indirect average relative acceleration, computed from MD simulation of 823,218 identical nanoparticles in 3-d case with volume fraction $\alpha = 0.45$ (left axis) and the radial distribution function $g(\hat{r})$ for the same system (right axis), with $\hat{\varepsilon} = 1$.

acceleration between particles i and j due to all other $N-2$ particles is extracted (Figure 5.5). In the dynamic case, an amplitude for the indirect average relative acceleration is similar to the amplitude of the direct average relative acceleration (Figure 5.1), when for static systems (Figure 5.3), an amplitude of indirect average acceleration is negligible. A periodic oscillation of the indirect relative acceleration with a decreasing of the peaks magnitude as $\hat{r}$ increases is an interesting result. It would be expected that as $\hat{r}$ increases an acceleration of i-th should decrease to 0 (Figure 5.1). However, because the indirect average relative acceleration is defined as integral over indirect acceleration and the radial distribution function $g(\hat{r})$ (Eq. 5.6), therefore if $g(\hat{r})$ does not monotonically decrease, it is possible that this integral does not equal 0 even when an indirect acceleration is very small. In the present case the radial distribution function is not a monotonic function (Figure 5.5), and a correlation between $\langle \Delta\hat{A}_i \rangle$ and $g(\hat{r})$ is observed. Thus, an oscillation of the indirect average relative acceleration occurs due to the oscillation of the radial distribution function $g(\hat{r})$.

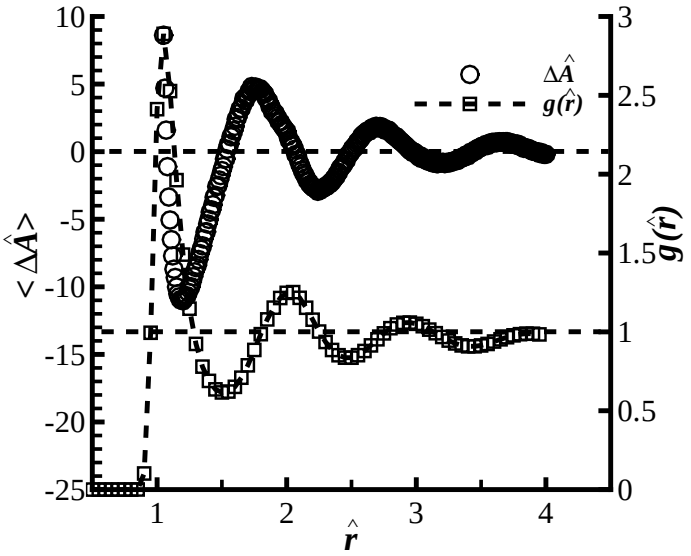

Figure 5.6 Total average relative acceleration computed from MD simulation of 823,218 identical particles in 3-d case with volume fraction $\alpha = 0.45$ (left axis) and the radial distribution function $g(\hat{r})$ for the same system (right axis), with $\hat{\varepsilon} = 1$.

For the same MD simulation a total relative acceleration is calculated according to Eq. 5.3 which is represented on Figure 5.6. These data show an oscillation around 0 when the analytical direct acceleration monotonically increases to a 0 after reaching a minimum (Figure 5.1). And a correlation between $\langle \Delta \hat{A} \rangle$ and $g(\hat{r})$ is observed in a similar way as in the case of the indirect average relative acceleration (Figure 5.5).

5.4 Relative Acceleration in a Mixture

5.4.1 Equilibrium System

In the case of a mixture of two kinds of particles at equilibrium, the system for MD simulations is similar to the one used for equilibrium simulations of uniform particles with the only difference that $10,000$ randomly selected particles are called A-type particles (nanoparticles) and the rest of the 813,218 particles are called B-type solvent molecules. Also the mass ratio

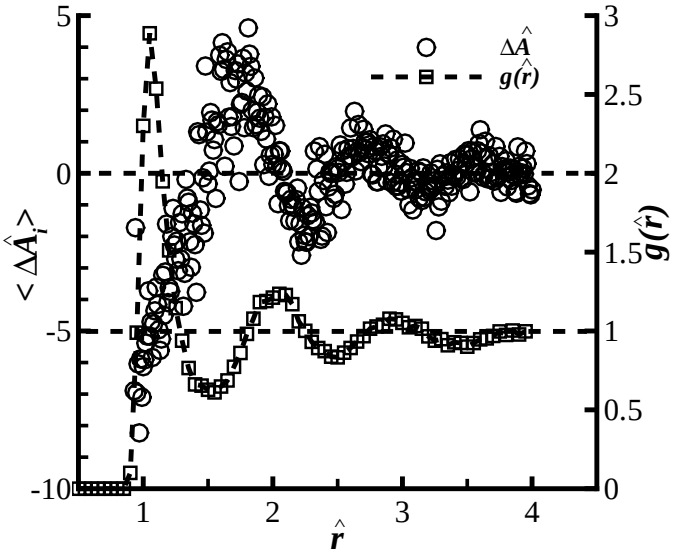

Figure 5.7 Indirect average relative acceleration, computed from MD simulation of 10,000 A-type particles and 813,218 B-type particles in 3-d case, with $m_A/m_B = 50$ and $\hat{\varepsilon}_{AA}/\hat{\varepsilon}_{BB} = 1$.

of A-type particles to B-type particle is $m_A/m_B = 50$. In this case, the total volume fraction of the system is $\alpha = 0.450$, the volume fraction of A-type particles is $\alpha_A = 0.005$, and for B-type particles $\alpha_B = 0.445$. An indirect average relative acceleration between the pair of A-type particles due to the presence of A-type and B-type particles is extracted from MD simulation of mixture of particles and is represented in Figure 5.7. The shape and magnitude of the indirect average relative acceleration in this case is very similar to the case of an equilibrium system with uniform particles (Figure 5.6). A radial distribution function $g(\hat{r})$ is similar for the mixture of particles and for the uniform particles case because interaction between particles remains the same. In the case of a mixture, due to the very low volume fraction of A-type particles, some spreading of the relative acceleration data is observed, when for the uniform particles case where the volume fraction is high the relative acceleration curve is relatively smooth. Thus by going from the ideal system to a more realistic one, the number of independent simulations should be increased to keep the same confidence interval for the

average relative acceleration data.

5.4.2 Aggregating System

Characteristics of an aggregating system are totally different from characteristics of an equilibrium one. In the equilibrium case, after reaching equilibrium, any state of the system in the future is statistically independent. Therefore, to improve statistical results, time averaging over different time steps can be applied. In the case of aggregation, the system does not reach an equilibrium state and to improve statistics an averaging over different independent simulations is required. This significantly increases the cost of computations.

To analyze the indirect average relative acceleration in case of aggregation, both MD and BD applications are used to generate aggregation systems. To simulate an aggregation with MD, the same initial system, as in the equilibrium case, is chosen with well-depth potentials corresponding to the aggregation case. Two aggregation systems are simulated with such reduced well-depth potentials: System 1 $\hat{\varepsilon}_{AA} = 4.0$, $\hat{\varepsilon}_{BB} = 1.0$, and $\hat{\varepsilon}_{AB} = \sqrt{4.0}$, and System 2 $\hat{\varepsilon}_{AA} = 8.0$, $\hat{\varepsilon}_{BB} = 1.0$, and $\hat{\varepsilon}_{AB} = \sqrt{8.0}$. To simulate aggregation with BD, the same system as in the MD case is used with no simulation of solvent molecules.

In the BD case the relative acceleration of A-A type particles due to the effect of A-type particles can be only computed. By the contrast in the MD case the relative acceleration of A-A type particles due to the effect of A-type particles, or B-type solvent molecules, or both A and B-type particles can be computed. Therefore, when the relative acceleration results are compared for MD and BD approaches, only the relative acceleration of A-A type particles due to effect of A-type particles can be directly compared.

Indirect average relative acceleration of A-A type particles by effect of both A-type and B-type particles is extracted from MD simulations for both systems (Figure 5.8). It is observed that indirect average relative acceleration data oscillates around zero for both systems. However, because these two systems generate different cluster structures (Figure 4.3) the indirect relative acceleration data are also different. Thus, for a system with $\hat{\varepsilon}_{AA} = 4$ the relative acceleration data (Figure 5.8a) decays to zero at a much smaller length scale than in the case of

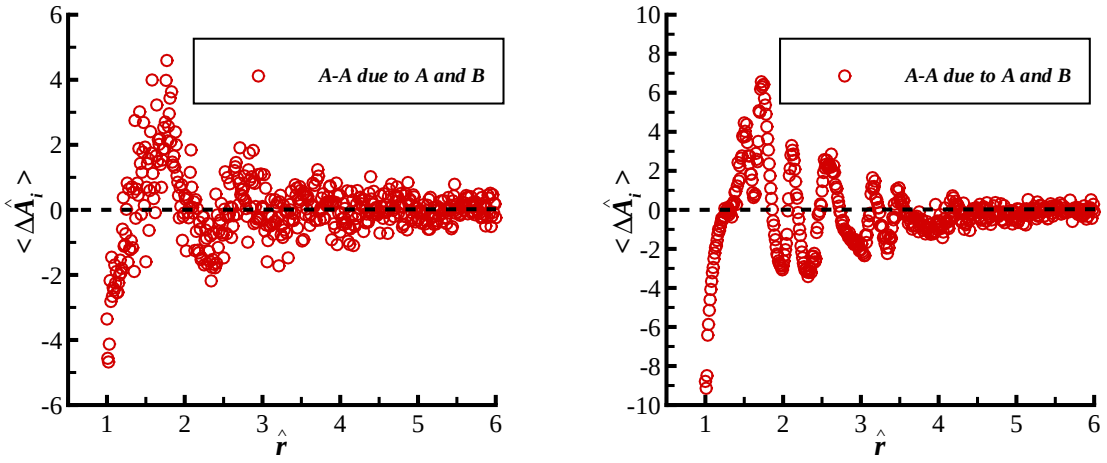

Figure 5.8 Indirect average relative acceleration of A-A type particles by effect of both A-type and B-type particles (10,000 A-type nanoparticles and 813,218 B-type nanoparticles) in 3-d case at time $\hat{t} = 329.8$, with $m_{nanop}/m_{solvent} = 50$: a) $\hat{\varepsilon}_{AA}/\hat{\varepsilon}_{BB} = 4.0$; b) $\hat{\varepsilon}_{AA}/\hat{\varepsilon}_{BB} = 8.0$.

$\hat{\varepsilon}_{AA} = 8$ (Figure 5.8b) which is related to the different scales of aggregates. Also, the number of oscillation cycles is significantly bigger for a system with a larger reduced well-depth value. These oscillations of an indirect average relative acceleration of A-A type particles identify that an attraction between pairs of A-A type particles occurs at some pair separation for the aggregating system. This provides the driving force for an aggregation to occur. This attraction can occur due to the effect of A-type particles and/or the effect of B-type particles. To identify which interaction is most significant, an indirect average relative acceleration of A-A type particles by effect of only A-type particles and due to effect of only B-type particles is computed for both systems. Data for the indirect average relative acceleration due to A-type particles only for both MD and BD simulations are represented in Figure 5.9. It can be seen that the indirect average relative acceleration calculated from MD simulations is significantly different for systems with different reduced well-depth values, while in the case of BD simulations such difference is minimal. Such different results obtained for MD and BD simulations can be explained by difference in the radial distribution function (Figure 4.2). By comparing

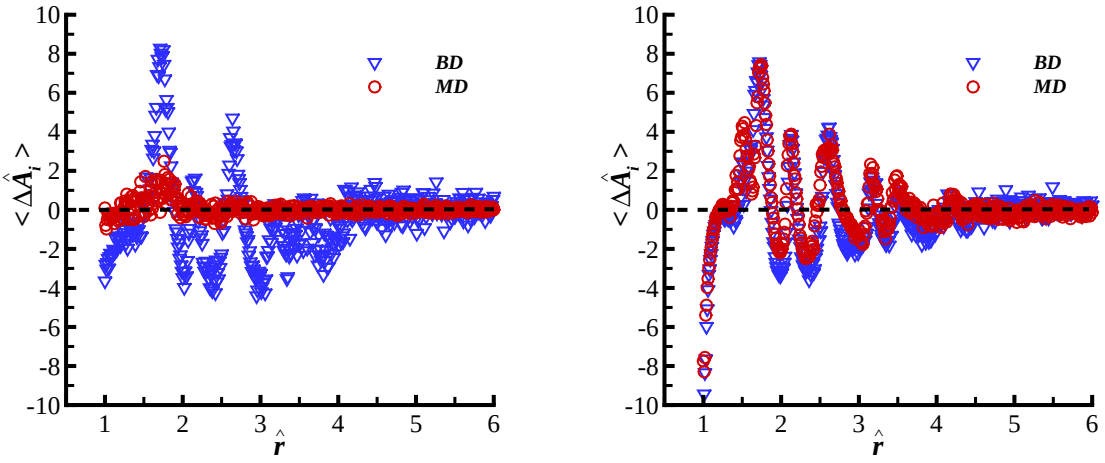

Figure 5.9 Indirect average relative acceleration of A-A type particles by effect of only A-type particles from MD simulation (10,000 A-type nanoparticles and 813,218 B-type nanoparticles) and BD simulation (10,000 A-type nanoparticles) in 3-d case with $m_{nanop}/m_{solvent} = 50$ at time $\hat{t} = 329.8$: a) $\hat{\varepsilon}_{AA}/\hat{\varepsilon}_{BB} = 4.0$; b) $\hat{\varepsilon}_{AA}/\hat{\varepsilon}_{BB} = 8.0$.

acceleration data for MD and BD simulations a very good matching of indirect acceleration data is observed for System 2 with $\hat{\varepsilon}_{AA}/\hat{\varepsilon}_{BB} = 8$, when for System 1 ($\hat{\varepsilon}_{AA}/\hat{\varepsilon}_{BB} = 4$) results are totally different. This behavior is related to the different aggregation regime for MD simulations. In the case of System 1 this is the RLA regime, and in System 2 this is the DLA regime.

To complete investigation of the indirect relative acceleration, an indirect relative acceleration between A-A type of particles due to the effect of only B-type particles is calculated (Figure 5.10). The magnitude of relative acceleration due to the effect of B-type particles is much smaller than due to the effect of A-type particles for System 2 (Figures 5.10b, 5.9b) when the DLA regime is dominant. However, when the RLA aggregation regime is dominant, A-type interaction and B-type interactions are both equally important (Figures 5.10a, 5.9a) and should be considered when improving aggregation modeling. Also, these results show that in case when the DLA regime is dominant (Figure 5.10b) the dependence of an indirect average

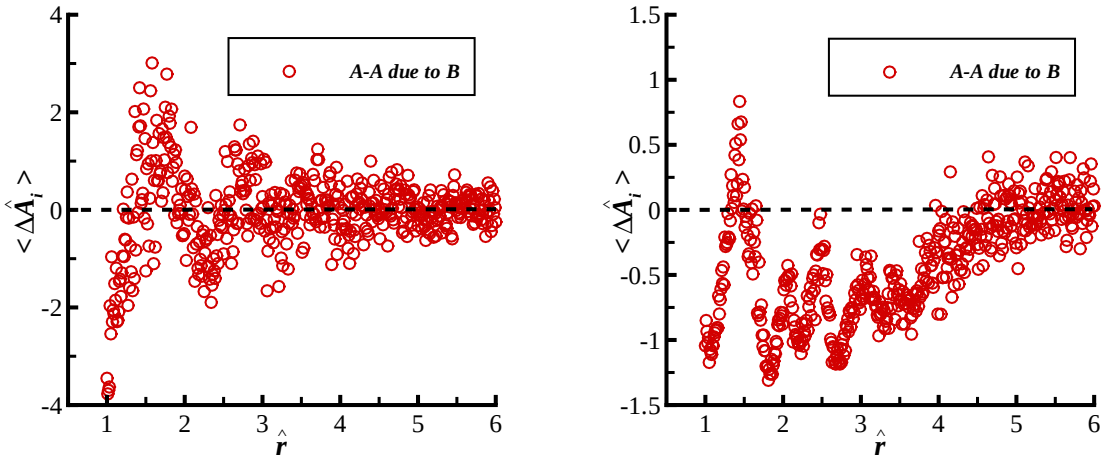

Figure 5.10 Indirect average relative acceleration of A-A particles by effect of only B particles (MD simulation of 10,000 A-type nanoparticles and 813,218 B-type nanoparticles) in 3-d case, with $m_{nanop}/m_{solvent} = 50$ at time $\hat{t} = 329.8$: a) $\hat{\varepsilon}_{AA}/\hat{\varepsilon}_{BB} = 4.0$; b) $\hat{\varepsilon}_{AA}/\hat{\varepsilon}_{BB} = 8.0$.

acceleration on the particle separation for the length scale of $\hat{r} < 5$ is observed, when in case of the RLA regime (Figure 5.10a) there is no dependence on $\hat{r}$.

From the analysis of an indirect average relative acceleration for aggregating systems the following conclusions can be made:

1. When the DLA regime is dominant in MD simulations, good match of the radial distribution function computed from the MD and BD simulations is observed (Figure 4.2b), which leads to good match of an indirect average relative accelerations (Figure 5.9b). As result, no improvement in the interaction potential is needed. However, the dependence of an indirect average relative acceleration on the separation distance $\hat{r}$ is observed for MD simulations (Figure 5.10b). Thus, to improve a BD model the dependence on $\hat{r}$ should be introduced into frictional and random terms in Langevin equation 3.2.

2. In case of the RDA regime, there is no dependence of the indirect average acceleration on $\hat{r}$ is observed (Figure 5.9). However, the radial distribution function does not match

for MD and BD simulations (Figure 4.2a), and therefore an indirect average acceleration does not match as well (Figure 5.9a). In this case an interaction potential should be modified to improve a BD model.

CHAPTER 6. CONCLUDING REMARKS

Two simulation approaches, molecular dynamics (MD) [7] and Brownian dynamics (BD) [21], are analyzed and compared with a view to accurately predicting aggregation of colloidal nanoparticles. The principal findings of this study are:

1. Molecular dynamics approach is not feasible to simulate an aggregation of colloidal nanoparticles for systems of physical sizes due to presence of very large number of solvent particles in such systems.

2. MD and BD comparison is possible only for model non-size separated systems and cannot be done for physical systems.

3. Reduction of position and velocity-Langevin equations to position-Langevin can be applied for physical system and is not justified for model system.

4. To satisfy accuracy requirements when simulating aggregation processes, a significant number of multiple independent simulations (MIS) is needed. The reason for this is that the aggregation process is evolving in time and it is impossible to improve statistics by performing time averaging as can be done for equilibrium systems. Therefore, accurate simulation of the aggregation process is computationaly demanding.

5. The extent of aggregation ξ, cluster size distribution (CSD) and radial distribution function $g(r)$ are important statistics which should be considered when analyzing the aggregation structure. The aggregation of colloidal nanoparticles in the BD approach is mainly controlled by the potential well-depth $\hat{\varepsilon}$, which identifies aggregation regimes, such as diffusion-limited aggregation, or reaction-limited aggregation. While the self-diffusion coefficent D_∞ just varies at the rate at which aggregation occures.

6. Light scattering analysis (LSA) is a powerful tool for analyzing the aggregate structure which allows us to extract such aggregation characteristics as the fractal dimension D_f for a range of aggregate length scales. The application of this tool is limited by requirements of a large dynamic range for precise measurements of D_f. This leads to requirements of large cluster sizes and small nanoparticles volume fraction (in order to shift the ideal gel point radius of gyration). Thus, a significant speed up of BD simulations is required.

7. For model systems with equal sizes of nanoparticles and solvent molecules, both MD and BD approaches predict similar aggregate structures with similar ξ, CSD, and $g(r)$ with high reduced well-depth potential ($\hat{\varepsilon} = 8$). For the same model systems but with $\hat{\varepsilon} = 4$, the aggregate structures predicted by BD do not match MD. The reason for this difference is that in both MD and BD approaches, the aggregation process depends on the $\hat{\varepsilon}$ value, which is related to the probability of two particles sticking together. Thus, with ($\hat{\varepsilon} = 8$) the DLA regime dominates for both MD and BD approaches, when with ($\hat{\varepsilon} = 4$) the RLA regime dominates in the MD approach and the DLA regime dominates in the BD approach.

8. A new method to match aggregation statistics obtained from MD and BD simulations is proposed. In this method the evolution of the second-order density for MD model is derived. The average relative acceleration between nanoparticle pairs is identified as an important link between MD and coarse-grain simulations such as BD in both DLA and RLA regimes.

Future work is suggested as follows:

1. It is important to perform a deep investigation of the $g(r)$ statistics with respect to the question if a $g(r)$ is a sufficient statistic to characterize the aggregation process. Also it is important to identify if a CSD is a sufficient statistic to characterize aggregation. These questions can be answered by finding the answers to the following questions: If $g(r)$ is given, can we compute CSD? And if CSD is given can we compute $g(r)$?

2. For more realistic cases, the systems with size separation of nanoparticles and solvent molecules should be simulated and compared for MD and BD. In this case the aggregation processes can change even if all other parameters will be the same due to changes in the self-diffusion coefficient of nanoparticles. Careful consideration of the model system is required in order to perform MD simulations; thus it will be hard to perform MD simulations with large size separation and a large number of nanoparticles.

3. Other coarse-graining methods such as dissipative particle dynamics (DPD) and stochastic rotational dynamics (SRD) can be implemented and compared with MD and BD results with respect to the accurate prediction of aggregation.

BIBLIOGRAPHY

[1] Roco, M. C. Nanoparticles and nanotechnology research. *J. Nanop. Rec.*, 1:1–6, 1999.

[2] Friedlander, S. K. Nanoparticles and their structures: the next generation. *J. Nanoparticle Rec.*, 1:159–160, 1999.

[3] Oh, C., and Sorensen C. M. The effect of overlap between monomers on the determination of fractal cluster morphology. *J. Colloid & Interf. Sci.*, 193:17–25, 1997.

[4] Oh, C., and Sorensen C. M. Structure factor of diffusion-limited aggregation clusters: Local structure and non-self-similarity. *Phys. Rev. E*, 57(1):784–790, 1998.

[5] Fry, D., Chakrabarti, A., Kim, W., and Sorensen C. M. Structural crossover in dense irreversibly aggregating particulate systems. *Phys. Rev. E*, 69:061401, 2004.

[6] Lattuada, M., Wu, H., Sandkuhler, P., Sefcik, J., and Morbidelli, M. Modelling of aggregation kinetics of colloidal systems and its validation by light scattering measurements. *Chem. Engin. Science*, 59:1783–1798, 2004.

[7] Ulberg, D. E., Churaev, N. V., Ilyin, V. V., and Malashenko, G. L. Molecular-dynamics simulation of the aggregation of colloidal particles. *Colloids & Surfaces A Physicoch. & Engin. Aspects*, 80:93–102, 1993.

[8] Witten, T. A., and Sander, L. M. Diffusion-limited aggregation, a kinetic critical phenomenon. *Phys. Rev. Lett.*, 47:1400–1403, 1981.

[9] Meakin, P., and Vicsek, T. Internal structure of diffusion-limited aggregates. *Phys. Rev. A*, 32(1):685–688,1985

[10] Meakin, P. Formation of fractal clusters and networks by irreversible diffusion-limited aggregation. *Phys. Rev. Lett.*, 51:1119–1122, 1983.

[11] Kolb, M., Botet, R., and Jullien, R. Scaling of kinetically growing clusters. *Phys. Rev. Lett.*, 51:1123–1126, 1983.

[12] Meakin, P. A historical introduction to computer models for fractal aggregates. *J. Sol-Gel Sci. & Tech.*, 15:97–117, 1999.

[13] Vold, M. J. Computer simulation of floc formation in a colloidal suspension. *J. Colloid & Sci.*, 18:684–695, 1963.

[14] Sutherland, D. N. A theoretical model of floc structure. *J. Colloid & Inter. Sci.*, 25:373–380, 1967.

[15] Jullien, R., and Kolb, M. Hierarchical model for chemically limited cluster-cluster aggregates. *Journal of Physics*, A17:L639–L643, 1984.

[16] Salazar, R., and Gelb, L. D. Off-lattice Dynamic Monte Carlo simulations of aggregation in one dimension. *Physica A*, 365:190–195, 2005.

[17] Hoogerbrugge, P. J., and Koelman, J. M. V. A. Simulating microscopic hydrodynamic phenomena with dissipative particle dynamics. *Europhys. Lett.*, 19:155–160, 1992.

[18] Español, P., and Warren, P. B. Statistical mechanics of dissipative particle dynamics. *Europhys. Lett.*, 30:191–196, 1995.

[19] Malevanets, A., Kapral, R. Mesoscopic model for solvent dynamics. *J. Chem. Phys.*, 110:8605–8613, 1999.

[20] Lee, S. H., and Kapral, R. Cluster structure and dynamics in a mesoscopic solvent. *Physica A*, 298:56–68, 2001.

[21] Ermak, D. L. Computer-simulation of charged-particles in solution .1. Technique and equilibrium properties. *J. Chem. Phys.*, 62:4189–4196, 1975.

[22] Sullivan, F., and Mountain, R. D. An efficient algorithm for the Brownian dynamics simulation of aggregation. *Comp. Phys. Comm.*, 42(1):43–49, 1986.

[23] Frenkel, D. and Smit, B. *Understanding Molecular Simulation*; Academic Press: San Diego, 2002.

[24] Pranami, G., Slipchenko, L., Lamm, M. H., and Gordon, M. S. (*in preparation*). A coarse-grained forcefield for polystyrene derived from the effective fragment potential.

[25] Adamovic, Li, H., Lamm, M. H., and Gordon, M. S. Modeling styrene-styrene interactions. *J. Phys. Chem. A*, 110:519525, 2006.

[26] Plimpton, S. J. Fast parallel algorithms for short-range molecular dynamics. *J. Comp. Phys.*, 117:1–19, 1995.

[27] Sorensen, C. M. Light scattering by fractal aggregates: A review. *Aerosol Sci. Tech.*, 35:648–687, 2001.

[28] Giro, A., and Guardia, E. Langevin and molecular dynamics simulations of Lennard-Jones liquids. *Mol. Phys.*, 55(5):1063–1074, 1985.

[29] Bos, M. T. A., and van Opheusden, J. H. J. Brownian dynamics simulation of gelation and aging in interacting colloidal systems. *Phys. Rev. E*, 53:5044-5050, 1996.

[30] Lodge, J. F. M., and Heyes, D. M. Brownian dynamics simulations of Lennard-Jones gas/liquid phase separation and its relevance to gel formation. *J. Chem. Soc. Faraday Trans.*, 93:437–448, 1997.

[31] Mellema, M., van Opheusden, J. H. J., and van Vliet, T. Relating colloidal particle interactions to gel structure using Brownian dynamics simulations and the Fuchs stability ratio. *J. Chem. Phys.*, 111:6129–6135, 1999.

[32] Puertas, A. M., Fernandez-Barbero, A., and de las Nieves, F. J. Structure factor scaling in colloidal charge heteroaggregation. *Eur. Phys. J. E*, 18:335–341, 2005.

[33] Cerda, J. J., Sintes, T., Sorensen, C. M., and Chakrabarti, A. Structure factor scaling in colloidal phase separation. *Phys. Rev. E*, 70:051405, 2004.

[34] Videcoq, A., Han, M., Abelard, P., Pagnoux, C., Rossignol, F., and Ferrando, R. Influence of the potential range on the aggregation of colloidal particles. *Physica A*, 374:507–516, 2007.

[35] Dickinson, E. Brownian dynamics with rotation-translation coupling. *J. Chem. Soc., Faraday Trans.* 81(2):591–601, 1985.

[36] Allen, M. P. Brownian dynamics simulation of a chemical reaction in solution. *Molecular Physics*, 40(5):1073–1087, 1980.

[37] Van Gunsteren, W. F., and Berendsen, H. J. C. Algorithms for brownian dynamics. *Molecular Physics*, 45(3):637–647, 1982.

[38] Turq, P., Lantelme, F., and Friedman, H. L. Brownian dynamics: Its application to ionic solutions. *The Journal of Chemical Physics*, 66(7):3039–3044, 1977.

[39] Ermak, D. L., and McCammon, J. A. Brownian dynamics with hydrodynamic interactions. *J.Chem. Phys.*, 69(4):1352–1360, 1978.

[40] Klyatskin, V. I. *Stochastic equations through the eye of the physicist*; Elsevier, 2005.

[41] Kloeden, P. E., Platen E. *Numerical solution of stochastic differential equations*; Springer-Verlag, 1992.

[42] Vicsek, T., and Family, F. Dynamic scaling for aggregation of clusters. *Phys. Rev. Lett.*, 52:1669–1672, 1984

[43] Fox, R. O. (private communication), 2006.

[44] Subramaniam, S., Pai, M. G. Transport of fluctuations in clustering particle systems: implications for constitutive models. *J. Fluid Mech.*, in review.

[45] Subramaniam, S. Statistical modeling of sprays using the droplet distribution function. *Physics of Fluids*, 13(3):624–642, 2001.

[46] Gardiner, C. W. *Handbook of Stochastic Methods*; Springer, 2004.

[47] Stoyan, D., and Stoyan, H. *Fractals, random shapes, and point fields : methods of geometrical statistics*; John Wiley&Sons, 1994.

APPENDIX A. Buchingham Pi Theory

Buchingham Pi Theory relies on the identification of variables involved in a process. Several steps shoul be procedeed to perform a nondimensional analysis.

1. List all the variables that govern the process.

   In our case we have: potential well depth ε, nanoparticle diameter σ, nanoparticle position $\mathbf{r}$, nanoparticle velocity $\mathbf{v}$, nanoparticle mass m, nanoparticle diffusion coefficient D_∞, $k_B T_{ref}$ where k_B is Boltzmann constant, reference temperature T_{ref}, time t, and particle number density λ. Thus all together there are $n = 9$ variables.

2. Between all variables in the system mark a few of them as "Repeating Variables". This step is most difficult in a dimensional analysis.

   In our case these are: σ, m, $k_B T_{ref}$ and $k = 3$

3. Define how many non-dimensional numbers is in system. In this case it is $n - k = 6$. Our problem has four non-dimensional numbers: Π_1, Π_2, Π_3, Π_4, Π_5, and Π_6.

4. Define the non-dimensional numbers by grouping the variables into $n-k$ groups. So each group has all the repeating variables and one non-repeating variable. For our problem we have:

$$\Pi_1 = \Pi_1(\sigma, m, k_B T_{ref}, \varepsilon) \tag{A.1}$$

$$\Pi_2 = \Pi_2(\sigma, m, k_B T_{ref}, D_\infty) \tag{A.2}$$

$$\Pi_3 = \Pi_3(\sigma, m, k_B T_{ref}, t) \tag{A.3}$$

$$\Pi_4 = \Pi_4(\sigma, m, k_B T_{ref}, \lambda) \tag{A.4}$$

$$\Pi_5 = \Pi_5(\sigma, m, k_B T_{ref}, \mathbf{r}) \quad (A.5)$$

$$\Pi_6 = \Pi_6(\sigma, m, k_B T_{ref}, \mathbf{v}) \quad (A.6)$$

Let

$$\Pi_1 = \sigma^a m^b (k_B T_{ref})^c \varepsilon \quad (A.7)$$

$$\Pi_2 = \sigma^d m^e (k_B T_{ref})^f D_\infty \quad (A.8)$$

$$\Pi_3 = \sigma^g m^h (k_B T_{ref})^i t \quad (A.9)$$

$$\Pi_4 = \sigma^j m^k (k_B T_{ref})^l \lambda \quad (A.10)$$

$$\Pi_5 = \sigma^m m^n (k_B T_{ref})^o \mathbf{r} \quad (A.11)$$

$$\Pi_6 = \sigma^p m^q (k_B T_{ref})^r \mathbf{v} \quad (A.12)$$

5. Express each variable in terms of its dimensions.

Variable	ε	σ	$\mathbf{r}$	$\mathbf{v}$	m	D_∞	$k_B T_{ref}$	t	λ
Dimension	ML^2/T^2	L	L	L/T	M	L^2/T	ML^2/T^2	T	$1/L^3$

Substituting these dimensions into Π_{1-6} at the previous step:

$$\Pi_1 = (L)^a (M)^b (ML^2/T^2)^c (ML^2/T^2) \quad (A.13)$$

$$\Pi_2 = (L)^d (M)^e (ML^2/T^2)^f (L^2/T) \quad (A.14)$$

$$\Pi_3 = (L)^g (M)^h (ML^2/T^2)^i (T) \quad (A.15)$$

$$\Pi_4 = (L)^j (M)^k (ML^2/T^2)^l (1/L^3) \quad (A.16)$$

$$\Pi_5 = (L)^m (M)^n (ML^2/T^2)^o (L) \quad (A.17)$$

$$\Pi_6 = (L)^p (M)^q (ML^2/T^2)^r (L/T) \quad (A.18)$$

or

$$a + 2c + 2 = 0;\ b + c + 1 = 0;\ -2c - 2 = 0$$

$$d + 2f + 2 = 0;\ e + f = 0;\ -2f - 1 = 0$$

$$g + 2i = 0;\ h + i = 0;\ -2i + 1 = 0$$

$$j + 2l - 3 = 0;\ k + l = 0;\ -2l = 0$$

$$m + 2o + 1 = 0;\ n + o = 0;\ -2o = 0$$

$$p + 2r + 1 = 0;\ q + r = 0;\ -2r - 1 = 0$$

Solving these equations yields,

$$a = 0;\ b = 0;\ c = -1$$

$$d = -1;\ e = 1/2;\ f = -1/2$$

$$g = -1;\ h = -1/2;\ i = 1/2$$

$$j = 3;\ k = 0;\ l = 0$$

$$m = -1;\ n = 0;\ o = 0$$

$$p = 0;\ q = 0.5;\ r = -0.5$$

Non-dimensional numbers become:

$$\hat{\varepsilon} = \frac{\varepsilon}{k_B T_{ref}} \tag{A.19}$$

$$\hat{D}_\infty = \frac{D_\infty}{\sigma}\sqrt{\frac{m}{k_B T_{ref}}} \tag{A.20}$$

$$\hat{t} = \frac{t}{\sigma}\sqrt{\frac{k_B T_{ref}}{m}} \tag{A.21}$$

$$\hat{\lambda} = \lambda\sigma^3 \tag{A.22}$$

$$\hat{\mathbf{r}} = \frac{\mathbf{r}}{\sigma} \tag{A.23}$$

$$\hat{\mathbf{v}} = \mathbf{v}\sqrt{\frac{m}{k_B T_{ref}}} \tag{A.24}$$

By introducing the velocity variance $\sigma_{v_\infty}^2 = k_B T_{ref}/m$ these equations reduce to

$$\hat{\varepsilon} = \frac{\varepsilon}{k_B T_{ref}} \tag{A.25}$$

$$\hat{D}_\infty = \frac{D_\infty}{\sigma\sigma_{v_\infty}} \tag{A.26}$$

$$\hat{t} = t\frac{\sigma}{\sigma_{v_\infty}} \tag{A.27}$$

$$\hat{\lambda} = \lambda\sigma^3 \tag{A.28}$$

$$\hat{\mathbf{r}} = \frac{\mathbf{r}}{\sigma} \tag{A.29}$$

$$\hat{\mathbf{v}} = \frac{\mathbf{v}}{\sigma_{v_\infty}} \tag{A.30}$$

It is clear that there are only three parameters that characterise the system (except position, velocity, and time), such as scaled particle number density $\hat{\lambda}$ (a particle volume fraction α can be used instead), a scaled nanoparticle diffusion coefficient $\hat{D}_\infty$, and a scaled potential well depth $\hat{\varepsilon}$.

APPENDIX B. Cluster Definition

In the present work clusters are defined by setting a clustering separation distance r_{cl}. Typical values for $r_{cl} = 1.2 \div 1.5\sigma$, where σ is the nanoparticle diameter. In the present work $r_{cl} = 1.2\sigma$ is chosen. The following algorithm for the definition of clusters in system of N nanoparticles is used:

1. Particle 1 is added to the list of the first cluster. Then, calculate a separation between particle 1 and the rest of $j = 2, \ldots, N$ particles. All the j particles which are separated by the distance $r_{1j} \leq r_{cl}$ are added to the list of the first cluster.

2. The separations between second particle in the list of the first cluster and the rest of particles in the system is calculated (except particles which already belong to the cluster). If separation is equal or smaller than r_{cl} then particle is added to the list of the first cluster. This procedure repeats untill all the particles in the list of the first cluster are checked.

3. The next particle after particle 1 which does not belong to the first cluster picked up and is added to the list of the second cluster. After this, procedure described in 1 and 2 repeats untill all the particles in the system will belong to clusters.

This is an easy and relatively fast method which allows to get a cluster size distribution (CSD) of N nanoparticles in the system. The main disadvantage of this method is dependence of the cluster size distribution on such external parameter as r_{cl}. Also, in this method a snapshot of system is analyzed which can give a different CSD than by analyzing a system in dynamic.

APPENDIX C. Evolution of the Second-Order Density for MD Model

Differentiating Eq. 5.1 with respect to time results in

$$\begin{aligned}
&\frac{\partial \rho^{(2)}(x_1, x_2, v_1, v_2, t)}{\partial t} = \\
&\langle -\sum_{i=1}^{N}\sum_{j=1}^{N} V_k^{(i)} \frac{\partial}{\partial x_{1k}} \delta(\mathbf{v}_1 - \mathbf{V}^{(i)})\delta(\mathbf{x}_1 - \mathbf{X}^{(i)})\delta(\mathbf{v}_2 - \mathbf{V}^{(j)})\delta(\mathbf{x}_2 - \mathbf{X}^{(j)}) \\
&-\sum_{i=1}^{N}\sum_{j=1}^{N} A_k^{(i)} \frac{\partial}{\partial v_{1k}} \delta(\mathbf{v}_1 - \mathbf{V}^{(i)})\delta(\mathbf{x}_1 - \mathbf{X}^{(i)})\delta(\mathbf{v}_2 - \mathbf{V}^{(j)})\delta(\mathbf{x}_2 - \mathbf{X}^{(j)}) \\
&-\sum_{i=1}^{N}\sum_{j=1}^{N} V_k^{(j)} \frac{\partial}{\partial x_{2k}} \delta(\mathbf{v}_1 - \mathbf{V}^{(i)})\delta(\mathbf{x}_1 - \mathbf{X}^{(i)})\delta(\mathbf{v}_2 - \mathbf{V}^{(j)})\delta(\mathbf{x}_2 - \mathbf{X}^{(j)}) \\
&-\sum_{i=1}^{N}\sum_{j=1}^{N} A_k^{(j)} \frac{\partial}{\partial v_{2k}} \delta(\mathbf{v}_1 - \mathbf{V}^{(i)})\delta(\mathbf{x}_1 - \mathbf{X}^{(i)})\delta(\mathbf{v}_2 - \mathbf{V}^{(j)})\delta(\mathbf{x}_2 - \mathbf{X}^{(j)})\rangle
\end{aligned} \tag{C.1}$$

where $V_k^{(i)}$ and $V_k^{(j)}$ represent the velocity of i-th and j-th nanoparticles correspondently along Cartesian coordinate k, and $A_k^{(i)}$ and $A_k^{(j)}$ represent the acceleration of i-th and j-th nanoparticles correspondently along Cartesian coordinate k. By substituting the relation

$$a \cdot \delta(a - b) = b \cdot \delta(a - b), \tag{C.2}$$

an expression is changing to

$$\begin{aligned}
&\frac{\partial \rho^{(2)}(x_1, x_2, v_1, v_2, t)}{\partial t} = \\
&\langle -\frac{\partial}{\partial x_{1k}}(v_{1k}\langle f_1' f_2'\rangle) - \frac{\partial}{\partial v_{1k}} \sum_{i=1}^{N}\sum_{j=1}^{N} (A_k^{(i)} \delta(\mathbf{v}_1 - \mathbf{V}^{(i)})\delta(\mathbf{x}_1 - \mathbf{X}^{(i)})\delta(\mathbf{v}_2 - \mathbf{V}^{(j)})\delta(\mathbf{x}_2 - \mathbf{X}^{(j)})) \\
&-\frac{\partial}{\partial x_{2k}}(v_{2k}\langle f_1' f_2'\rangle) - \frac{\partial}{\partial v_{2k}} \sum_{i=1}^{N}\sum_{j=1}^{N} (A_k^{(j)} \delta(\mathbf{v}_1 - \mathbf{V}^{(i)})\delta(\mathbf{x}_1 - \mathbf{X}^{(i)})\delta(\mathbf{v}_2 - \mathbf{V}^{(j)})\delta(\mathbf{x}_2 - \mathbf{X}^{(j)}))\rangle
\end{aligned} \tag{C.3}$$

By defining the following function in phase space:

$$\langle A_k^{(i)} | x_1, x_2, v_1, v_2, t\rangle \rho^{(2)}(x_1, x_2, v_1, v_2, t) = \tag{C.4}$$

$$\sum_{i=1}^{N}\sum_{j=1}^{N}(A_k^{(i)}\delta(\mathbf{v}_1-\mathbf{V}^{(i)})\delta(\mathbf{x}_1-\mathbf{X}^{(i)})\delta(\mathbf{v}_2-\mathbf{V}^{(j)})\delta(\mathbf{x}_2-\mathbf{X}^{(j)}))$$

An expression for the second-order density is

$$\begin{aligned}&\frac{\partial\rho^{(2)}(x_1,x_2,v_1,v_2,t)}{\partial t}=-\frac{\partial}{\partial x_{1k}}\Big(v_{1k}\rho^{(2)}(x_1,x_2,v_1,v_2,t)\Big) \\ &-\frac{\partial}{\partial x_{2k}}\Big(v_{2k}\rho^{(2)}(x_1,x_2,v_1,v_2,t)\Big)-\frac{\partial}{\partial v_{1k}}\Big(\langle A_k^{(i)}|x_1,x_2,v_1,v_2,t\rangle\rho^{(2)}(x_1,x_2,v_1,v_2,t)\Big) \\ &-\frac{\partial}{\partial v_{2k}}\Big(\langle A_k^{(j)}|x_1,x_2,v_1,v_2,t\rangle\rho^{(2)}(x_1,x_2,v_1,v_2,t)\Big)\end{aligned} \tag{C.5}$$

Now, by changing variables in the following way $\mathbf{r}=\mathbf{x}_2-\mathbf{x}_1$ and $\mathbf{w}=\mathbf{v}_2-\mathbf{v}_1$, the final expression can be written in the vector form as

$$\begin{aligned}&\frac{\partial\rho^{(2)}(\mathbf{r},\mathbf{w},t)}{\partial t}+\frac{\partial}{\partial\mathbf{r}}\Big(\mathbf{w}\rho^{(2)}(\mathbf{r},\mathbf{w},t)\Big) \\ &-\frac{\partial}{\partial\mathbf{w}}\Big(\langle\mathbf{A}^{(i)}|\mathbf{r},\mathbf{w},t\rangle\rho^{(2)}(\mathbf{r},\mathbf{w},t)\Big)+\frac{\partial}{\partial\mathbf{w}}\Big(\langle\mathbf{A}^{(j)}|\mathbf{r},\mathbf{w},t\rangle\rho^{(2)}(\mathbf{r},\mathbf{w},t)\Big)=0\end{aligned} \tag{C.6}$$

And finally,

$$\frac{\partial\rho^{(2)}(\mathbf{r},\mathbf{w},t)}{\partial t}+\nabla_{\mathbf{r}}\cdot\Big(\mathbf{w}\rho^{(2)}(\mathbf{r},\mathbf{w},t)\Big)+\nabla_{\mathbf{w}}\cdot\Big(\langle\Delta\mathbf{A}|\mathbf{r},\mathbf{w},t\rangle\rho^{(2)}(\mathbf{r},\mathbf{w},t)\Big)=0 \tag{C.7}$$

where $\mathbf{r}$ represents the pair separation vector, $\mathbf{w}$ represents the relative velocity vector, and $\langle\Delta\mathbf{A}|\mathbf{r},\mathbf{w},t\rangle$ represents the expected relative acceleration $\Delta\mathbf{A}=\mathbf{A}^{(j)}-\mathbf{A}^{(i)}$ conditional on relative velocity and pair separation.

In Molecular Dynamics case, an acceleration, experienced by i-th particle is

$$\mathbf{A}_{MD}^{(i)}=\frac{d\mathbf{V}^{(i)}}{dt}=\frac{\mathbf{F}_{MD}^{(i)}}{m} \tag{C.8}$$

where $\mathbf{F}_{MD}^{(i)}$ is the force that i-th particle experienced due to an interaction with all other particles.

Thus, in MD case an expression for the evolution of the second order density is

$$\frac{\partial\rho_{MD}^{(2)}(\mathbf{r},\mathbf{w},t)}{\partial t}+\nabla_{\mathbf{r}}\cdot\Big(\mathbf{w}\rho_{MD}^{(2)}(\mathbf{r},\mathbf{w},t)\Big)+\nabla_{\mathbf{w}}\cdot\Big(\langle\Delta\mathbf{A}_{MD}|\mathbf{r},\mathbf{w},t\rangle\rho_{MD}^{(2)}(\mathbf{r},\mathbf{w},t)\Big)=0 \tag{C.9}$$

where $\Delta\mathbf{A}_{MD}=\mathbf{A}_{MD}^{(j)}-\mathbf{A}_{MD}^{(i)}$.

ACKNOWLEDGEMENTS

I would like to take this opportunity to express my sincere thanks and deep appreciation to those who helped me with various aspects of conducting research and the writing of this thesis. First and foremost, I would like to thank Dr. Shankar Subramaniam for his constant guidance, encouragement, patience and support throughout this research and the writing of this thesis. His scientific knowledge, technical skills and enlightened views on the research process has left a deep impression on me. How fortunate I am to have been a graduate student in his laboratory.

I would also like to thank my POS committee members for their efforts and contributions to this work: Dr. Rodney Fox, Dr. Dennis Vigil, and Dr. Pranav Shrotriya.

My special appreciation extends to all my lab-mates: Ragul Garg, Madhu Pai, Xu Ying, Wang Wen, Vidyapati, and Tenneti Sudheer. Thank you for your friendship and essential support. You made my life in the lab comfortable and enjoyable.

My thanks to the Department of Mechanical Engineering and its professional and administrative staff, especially Adin Mann, Marti Steelman, Char Kravinsky, Allison Mickelson, Hap Steed, and Nate Jensen their flawless and cheerful assistance during the past years.

Finally, I would like to extend love and thanks to my family, especially to my wife Svitlana for her love, patience and enduring support during my graduate studies at ISU. I am grateful for my mother and my mother-in-law for their help with caring for our daughter Alina, whose entry into our lives gave us extra motivation to pursue our dreams.